Redox Biology 48 (2021) 102201

Contents lists available at ScienceDirect

Redox Biology

journal homepage: www.elsevier.com/locate/redox

LRPPRC regulates redox homeostasis via the circANKHD1/FOXM1 axis to enhance bladder urothelial carcinoma tumorigenesis

Wen-Su Wei [a,b,1], Ning Wang [a,b,1], Min-hua Deng [a,b,1], Pei Dong [a,b,1], Jian-ye Liu [c,1], Zhen Xiang [d], Xiang-Dong Li [a,b], Zhi-yong Li [a,b], Zhen-hua Liu [a,b], Yu-lu Peng [a,b], Zhen Li [a,b], Li-Juan Jiang [a,b], Kai Yao [a,b], Yun-lin Ye [a,b], Wen-hua Lu [a], Zhi-Ling Zhang [a,b], Fang-Jian Zhou [a,b], Zhuo-Wei Liu [a,b,***], Dan Xie [a,e,**], Chun-ping Yu [a,b,*]

[a] State Key Laboratory of Oncology in South China, Sun Yat-Sen University Cancer Center, Collaborative Innovation Center for Cancer Medicine, No. 651, Dongfeng Road East, Guangzhou, PR China
[b] Department of Urology, Sun Yat-Sen University Cancer Center, No. 651, Dongfeng Road East, Guangzhou, PR China
[c] Department of Urology, Xiangya Third Hospital, No. 106, 2nd Zhongshan Road, Changsha, PR China
[d] Fudan University Shanghai Cancer Center, Shanghai, 200032, PR China
[e] Department of Pathology, Sun Yat-sen University Cancer Center, Guangzhou, PR China

ARTICLE INFO

Keywords:
Urothelial carcinoma of the bladder
LRPPRC
circRNA
FOXM1
ROS

ABSTRACT

Reactive oxygen species (ROS) which are continuously generated mainly by mitochondria, have been proved to play an important role in the stress signaling of cancer cells. Moreover, pentatricopeptide repeat (PPR) proteins have been suggested to take part in mitochondrial metabolism. However, the mechanisms integrating the actions of these distinct networks in urothelial carcinoma of the bladder (UCB) pathogenesis are elusive. In this study, we found that leucine rich pentatricopeptide repeat containing (LRPPRC) was frequently upregulated in UCB and that it was an independent prognostic factor in UCB. We further revealed that LRPPRC promoted UCB tumorigenesis by regulating the intracellular ROS homeostasis. Mechanistically, LRPPRC modulates ROS balance and protects UCB cells from oxidative stress via mt-mRNA metabolism and the circANKHD1/FOXM1 axis. In addition, the SRA stem-loop interacting RNA binding protein (SLIRP) directly interacted with LRPPRC to protect it from ubiquitination and proteasomal degradation. Notably, we showed that LRPPRC modulated the tumorigenesis of UCB cells in a circANKHD1-FOXM1-dependent manner. In conclusion, LRPPRC exerts critical roles in regulating UCB redox homeostasis and tumorigenesis, and is a prognostic factor for UCB; suggesting that LRPPRC may serve as an exploitable therapeutic target in UCB.

Abbreviations: UCB, Urothelial carcinoma of the bladder; NMIBC, non-muscle invasive bladder cancer; MIBC, muscle invasive bladder cancer; PFS, progression-free survival; OS, overall survival; miRNA, microRNA; circRNA, circular RNA; RT-qPCR, real time quantitative PCR; FISH, fluorescence *in situ* hybridization; WB, western blot; IP, immunoprecipitation; IHC, Immunohistochemistry; ROS, Reactive oxygen species; TCGA, The Cancer Genome Atlas; siRNA, short interfering RNA; shRNA, short hairpin RNA; ΔΨm, mitochondrial membrane potential; OXPHOS, oxidative phosphorylation; ETC, electron transport chain; TCA, tricarboxylic acid; mt-mRNAs, mRNAs encoded by mitochondrial; DEGs, The differentially expressed genes.

* Corresponding author. State Key Laboratory of Oncology in South China; Collaborative Innovation Center for Cancer Medicine; Sun Yat-sen University Cancer Center, 510060, Guangzhou, China.

** Corresponding author. State Key Laboratory of Oncology in South China; Collaborative Innovation Center for Cancer Medicine; Sun Yat-sen University Cancer Center, 510060, Guangzhou, China.

*** Corresponding author. State Key Laboratory of Oncology in South China; Collaborative Innovation Center for Cancer Medicine; Sun Yat-sen University Cancer Center, 510060, Guangzhou, China.

E-mail addresses: liuzhw@sysucc.org.cn (Z.-W. Liu), xiedan@sysucc.org.cn (D. Xie), yuchp@sysucc.org.cn (C.-p. Yu).

[1] WSW, NW, MHD, PD and JYL contributed equally to this work.

https://doi.org/10.1016/j.redox.2021.102201
Received 26 October 2021; Received in revised form 25 November 2021; Accepted 26 November 2021
Available online 27 November 2021

1. Introduction

Urothelial carcinoma of the bladder (UCB) is the tenth most frequent cancer worldwide in both sexes combined. It has the highest prevalence among urinary tract cancers, with an estimated 549,000 new cases and 200,000 deaths in 2018 worldwide [1]. Although current therapies, i.e. transurethral resection (TUR) combined with adjuvant intravesical treatment, are effective in treating non-muscle invasive bladder cancer (NMIBC), which accounts for around 75% of all cases of UCB, therapies for the advanced cases are less efficient [2]. The remaining 25% of patients are usually diagnosed as muscle invasive bladder cancer (MIBC) and commonly suffer from regional and/or systemic dissemination [3]. The management of MIBC or very-high-risk NMIBC involves radical cystectomy and cisplatin-based chemotherapy [4]. Unfortunately, treatment failure is observed in more than 50% of the patients due to the associated comorbidities and inherent or acquired chemoresistance [5,6]; leading to poor prognosis, with a median progression-free survival (PFS) and overall survival (OS) of ~8 and 14 months, respectively [7]. Therefore, a better understanding of the mechanisms involved in UCB tumorigenesis and/or progression is required for developing more efficient treatment strategies.

Mitochondria have multifaceted functions in normal physiology. Apart from ATP production, they also act as cellular stress sensors which allow cellular adaptation. However, this can be a double-edged sword function because in harsh conditions of the tumor microenvironment, such as hypoxia, nutrient depletion and during cancer treatments, this can make cancer cells more flexible to adapt, grow and survive [8,9]. Reactive oxygen species (ROS), which are continuously generated in cells, mainly by mitochondria, have been recognized as a crucial mediator of multiple cellular processes such as signal transduction, proliferation and apoptosis [10]. It has been suggested that low/medium levels of ROS enhance cell survival and lead to genetic instability, but excessive ROS levels result in stimulation of cell death pathways [11]. Advances in our understanding of the essential role of mitochondrial processes in cancer could highlight their potential as a target for UCB therapy.

Pentatricopeptide repeat (PPR) proteins are a large family of RNA-binding proteins characterized by a canonical 35 residue repeat motif [12]. Only seven PPR proteins are found in humans, all localized in mitochondria, and are involved in multiple cellular processes, especially in RNA metabolism [12,13]. The biological significance of PPR proteins is highlighted by the discovery of their important roles in mitochondrial gene expression and energy metabolism. For instance, mitochondrial RNA polymerase (POLRMT) regulates mitochondrial mRNA (mt-mRNA) transcription [14,15]; pentatricopeptide repeat domain 1 (PTCD1), pentatricopeptide repeat domain 2 (PTCD2), and protein only RNase P catalytic subunit (KIAA0391) are involved in mt-mRNA processing [16–18]; LRPPRC regulates mt-mRNA maturation and stability [19–21], and KIAA0391 and pentatricopeptide repeat domain 3 (PTCD3) are involved in mitochondrial protein synthesis [22,23]. Recently, a growing number of PPRs have been verified to be important regulators in oncogenic processes. For example, POLRMT was found to participate in the progression of non-small cell lung cancer cell growth via the regulation of mt-RNA polymerase [24]. Several studies have reported that LRPPRC, which regulates the expression of all mt-mRNAs, is frequently overexpressed in multiple cancer tissues [25,26]. The dysregulation of LRPPRC may initiate carcinogenesis and inhibit the apoptosis of cancer cells [26]. To date, however, the significance of PPRs abnormalities in UCB pathogenesis has not been clearly elucidated.

In this present study, we identified LRPPRC as a potentially critical oncogenic factor in UCB pathogenesis by analyzing The Cancer Genome Atlas (TCGA) UCB project data and high-throughput RNA sequencing data from the Sun Yat-Sen University Cancer Center (SYSUCC; Guangzhou, China). Our data showed that overexpression of LRPPRC was an independent prognostic factor in UCB. *In vitro* and *in vivo* assays revealed that knockdown of LRPPRC in UCB cells significantly inhibited cell proliferation and/or induced cell apoptosis by increasing ROS levels in UCB cells. According to our results, SRA stem-loop interacting RNA binding protein (SLIRP) forms a stable complex with LRPPRC to protect it from degradation, which substantially enhances the function of LRPPRC in UCB cells. Importantly, we showed for the first time that LRPPRC modulates ROS balance and protects UCB cells from oxidative stress via mt-mRNA metabolism and the circANKHD1/FOXM1 axis; thereby resulting in UCB tumorigenesis. Clinically, the expression of LRPPRC positively correlated with circANKHD1 and FOXM1; all of which show that LRPPRC exerts a critical role in ROS metabolism and UCB tumorigenesis.

2. Materials and methods

2.1. Patients and tissue samples

In this study, 408 UCB patients with PPRs gene RNA sequencing data and detailed clinical information were retrieved from the TCGA database (https://cancergenome.nih.goc/). Among them, 19 cases were paired with adjacent non-neoplastic bladder tissues. Deep-sequencing data of 22 pairs of UCB and matched adjacent normal bladder tissues were obtained from the Gene Expression Omnibus database (GSE133671). For Western blot analyses, the cancer tissues and corresponding normal matched tissues from 10 UCB patients who had received radical cystectomy at SYSUCC in 2020 were used. For immunohistochemistry (IHC) analyses, the paraffin-embedded tumor tissues of 224 UCB patients who had undergone radical cystectomy at SYSUCC, consecutively from 2007 to 2017, were used. The clinical information of the UCB patients is summarized in Supplementary Table 1. The tumor stage and tumor grade were defined using the World Health Organization criteria and the seventh edition of the TNM classification of Union for International Cancer Control (UICC; 2010). All of the patients were followed up on a regular basis. Overall survival (OS) time was determined from the date of surgery to the date of death, and it was censored at the date of the last follow-up visit for survivors.

Thirty UCB tissue samples and paired adjacent non-neoplastic tissue samples were snap-frozen in liquid nitrogen upon collection for quantitative real-time polymerase chain reaction (qRT-PCR) assays. This study was approved by the Institutional Review Board of SYSUCC. All studies involving human research participants were blinded.

2.2. Immunohistochemistry

IHC was performed as previously described [27]. Briefly, the slides prepared for IHC were cut at a 3-μm thickness from the paraffin-embedded tissues. The tissue sections were then heated at 50 °C for 4 h, deparaffinized, and rehydrated using 100% xylene three times followed by 100%, 95%, 75% and 50% ethanol immersion for 5 min each. Endogenous peroxidase activity was blocked with 0.3% hydrogen peroxide for 15 min. For antigen retrieval, the slides were boiled in Tris (hydroxymethyl) aminomethane-EDTA buffer (pH 8.0) in a pressure cooker for 10 min. Nonspecific binding was blocked with 10% normal rabbit serum for 30 min. After washing in PBS twice for 2 min each, 100 μL of blocking buffer was added on each section and incubated at room temperature for 25 min. Then, 100 μL of primary antibody diluted in 1% BSA was added on each section. The slides were incubated with primary antibodies against LRPPRC (dilution: 1:200), FOXM1 (dilution: 1:200), and PRDX3 (dilution: 1:100) overnight at 4 °C in a moist chamber. Then, they were washed twice in PBS for 2 min and incubated with a biotinylated secondary antibody (100 μL per section) for 30 min at room temperature. Immunostaining was performed using the Envision System with diaminobenzidine (Dako).

The HALO image analysis platform (Indica Labs, Corrales, New Mexico, USA) was used for quantitative assessment of IHC staining for LRPPRC, FOXM1 and PRDX3 [28–30]. Briefly, stained nuclei were automatically detected by the software and nuclear regions were

expanded to quantify cytoplasmic LRPPRC, FOXM1 or PRDX3 staining, followed by calculation of the percentage of cells with different levels of protein expression intensity, namely, no staining, weak staining, moderate staining, and strong staining [30]. The IHC scores were automatically calculated using the HALO software. Low and high LRPPRC expression was determined on the basis of the median score (5.2) of all samples as a cut-off. All patients were then classified into two groups, namely, the low LRPPRC expression group (IHC score $\leq$5.2; n = 112), and the high LRPPRC expression group (IHC score >5.2; n = 112).

2.3. Cell cultures

The SV-HUC-1, T24, J82, TCC-SUP, UM-UC-3, SW-780, 5637 and RT4 cell lines were purchased from the American Type Culture Collection (ATCC). T24, J82, and 5637 cells were cultured in RPMI-1640 medium (Invitrogen, Carlsbad, USA) with 10% fetal bovine serum (HyClone, USA). SV-HUC-1, SW-780, TCC-SUP, UM-UC-3 and RT4 cells were cultured in DMEM (Invitrogen, Carlsbad, USA) with 10% fetal bovine serum (HyClone, USA). All cells were grown in a humidified incubator at 37 °C with 5% CO_2.

2.4. RNA interference and transfection

Short interfering RNA (siRNA) duplexes were synthesized by RiboBio (Guangzhou, China). The short hairpin RNAs (shRNAs) used for RNA interference were obtained from GeneCopoeia (MD, USA). The target sequences are listed in Supplementary Data 1.

2.5. Plasmid construction and miRNA mimics

pcDNA 3.1-FLAG-tagged human LRPPRC and pCDH-CMV-GFP-tagged human SLIRP overexpression plasmids were purchased from Vigene Biosciences (Maryland, USA). miR-671-5p and miR-507 mimics were obtained from RiboBio (Guangzhou, China). The overexpression plasmid (pLC5-ciR) of circANKHD1 was purchased from Geneseed (Guangzhou, China). The circANKHD1 sequence containing the miR-671-5p and miR-507 binding sites was inserted into the pmirGLO vector, and the binding sites of miR-671-5p and miR-507 were mutated as a template to generate pmirGLO-circANKHD1-Mut671 and pmirGLO-circANKHD1-Mut507 (GeneCreate, Wuhan, China), respectively. Plasmid transfection was performed using Lipofectamine 3000 (Invitrogen, Carlsbad, USA). Lentivirus production and infection were performed with a Lenti-Pac HIV package kit and concentrated with Concentration of lentiviral particles (GeneCopoeia). Puromycin was used to select stable cells.

2.6. Antibodies

The antibodies used for this study were purchased from the following commercial sources: anti-LRPPRC (Western blot; sc-166178, Santa Cruz, Texas, USA); anti-LRPPRC (co-immunoprecipitation [co-IP] and IHC; 21175-1-AP, Proteintech, Chicago, USA); anti-SLIRP (Western blot, co-IP and IHC; 26006-1-AP, Proteintech, Chicago, USA); anti-Flag (Western blot and co-IP; 8146, CST, Boston, USA); anti-FOXM1 (Western blot and IHC; 13147-AP, Proteintech, Chicago, USA); anti-PRDX3 (Western blot and IHC; 10664-AP, Proteintech, Chicago, USA); anti-MnSOD (Western blot; S5069, Sigma Aldrich, USA); anti-Catalase (Western blot; 21260-1-AP, Proteintech, Chicago, USA); anti-Cleaved CASP9; anti-Cleaved CASP3; anti-Cleaved PARP (Western blot; 9929, CST, Boston, USA); anti-CASP8 (Western blot; 4790, CST, Boston, USA); anti-BCL2 (Western blot; 4223, CST, Boston, USA); anti-BAX (Western blot; 5023, CST, Boston, USA); and anti-α-Tubulin (Western blot; 66031-1-Ig, Proteintech, Chicago, USA).

2.7. Western blotting

Total proteins were extracted using a lysis buffer, and equal amounts of protein lysates were separated on 12% or 10% SDS-PAGE and transferred to PVDF membranes (Millipore, Massachusetts, USA). After blocking and incubating with the indicated primary antibodies at 4 °C, the membranes were washed in TBST thrice for 5 min. Then, they were hybridized with anti-mouse (PR30012, Proteintech, Chicago, USA) or anti-rabbit (PR30011, Proteintech, Chicago, USA) IgG-linked horseradish peroxidase secondary antibodies for 1 h at room temperature. Finally, the membranes were visualized by enhanced chemiluminescence (Thermo Fisher Scientific, USA) and analyzed using the ImageJ software. The following antibodies and dilutions were used: anti-LRPPRC (dilution: 1:1000); anti-SLIRP (dilution: 1:1000); anti-FOXM1 (dilution: 1:1000); anti-PRDX3 (dilution: 1:1000); anti-MnSOD (dilution: 1:1000); anti-Catalase (dilution: 1:2000); anti-FLAG (dilution: 1:1000); anti-BCL2 (dilution: 1:1000); anti-BAX (dilution: 1:1000); anti-Cleaved CASP9 (dilution: 1:1000); anti-Cleaved CASP3 (dilution: 1:1000); anti-Cleaved PARP (dilution: 1:1000); CASP8 (dilution: 1:1000); and anti-α-Tubulin (dilution: 1:5000).

2.8. qRT-PCR

Total RNA was extracted using TRIzol reagent (Invitrogen, Carlsbad, USA). The mRNA (2 mg) was reverse-transcribed to generate cDNA using a PrimeScript RT reagent kit (Takara) in accordance with the manufacturer's protocol, and a portion of that was used for PCR assay. For qRT-PCR reactions, SYBRGREEN (Roche, Basel, Switzerland) and ABI7900HT Fast Real-Time PCR system (Applied Biosystems, CA, USA) were used. The primer sequences are listed in Supplementary Data 1. For the analysis of qRT-PCR data, the "relative expression" of each product was normalized to β-actin and were analyzed using the Relative Quantification ($^{\Delta\Delta}$CT) method, calculated by $2^{-\Delta\Delta CT}$ and further presented as "fold change" compared to relative controls.

2.9. Cell proliferation and oncogenic assays

For cell growth assays, the cells were seeded in 96-well plates at a density of 1×10^3 cells/well, and cell growth rate was assessed using the CCK8 kit (Dojindo Laboratories). For colony-formation assays, 300 cells were seeded in 6-well plates and cultured at 37 °C with 5% CO_2 for 2 weeks. After fixation with 4% formaldehyde for 15 min, the cells were stained using crystal violet staining. For 5-ethynyl-20 deoxyuridine (EdU) assays, after the cells were seeded in a well and cultured for 24 h, newly synthesized DNA of the cells were assessed using a Cell-Light EdU DNA Cell Proliferation Kit obtained from RiboBio (Guangzhou, China), in accordance with the manufacturer's instructions. The positive rate of EdU incorporation was counted as the ratio of EdU-positive cells to total cells.

2.10. Apoptosis analysis

After dissociation by 0.25% trypsin-EDTA and harvesting by centrifugation, the cells were washed thrice with phosphate-buffered saline (PBS). An Annexin V Apoptosis Detection Kit (Thermo Fisher Scientific, USA) was used to determine apoptosis in accordance with the manufacturer's instructions. Briefly, the cells were resuspended in 100 μL binding buffer containing 5 μL of FITC-conjugated Annexin V antibody, and incubated for 15 min at room temperature. Then, they were washed and resuspended in a 200 μL binding buffer with 5 μL of propidium iodide (PI). Finally, the cells were analyzed using the CytoFlex (Beckman Coulter) flow cytometry and FlowJo software (Treestar).

2.11. RNA-SEQ and circRNA-SEQ

RNAs from control or sh-LRPPRC T24 cells were used to generate

mRNA sequencing libraries using the NEB Next Ultra RNA Library Prep Kit for Illumina (NEB, USA). The purified library products were evaluated using the Agilent 2200 TapeStation and Qubit 2.0 (Life Technologies, USA) and then sequenced on HiSeq 3000 at RiboBio Co., Ltd. (Guangzhou, China). FPKM (Fragments Per Kilobase of transcript per Million mapped reads) was calculated and mapped to the hg19 genome with HISAT2 (Johns Hopkins University, USA). For the analysis of RNA-SEQ data, the results were presented as "fold change" relative to T24-NC cells. Cuffdiff was used to analyze the differentially expressed genes (DEGs) between samples, with a cutoff fold change of 1.5. Genes with $|\log2(\text{fold change})|>1$ were selected for KEGG and GO analysis.

CIRI2 and CIRCexplorer2 were used to identify and quantify the expression profile of circRNAs. If a circRNA was detected by both algorithms, it was considered an identified circRNA. Back-spliced junction reads identified in CIR2 were combined and scaled to RPM (Reads Per Million mapped reads, BWA-MEM mapping) to quantify every circRNA. Reads were mapped to human reference genome GRCh37/hg19 by BWA-MEM or Tophat.

2.12. RNase R treatment and actinomycin D treatment assay

After the extraction of total RNA, 2 μg RNA was incubated with 6 U RNase R (Epicentre Technologies, Madison, WI, USA) for 15 min at 37 °C. T24 cells were seeded onto 6-well plates until they reached 60% confluence, then, the cells were treated with 5 μg/mL actinomycin D or DMSO, and RNA was extracted at indicated time points. Next, the RNA expression levels of ANKHD1 and circANKHD1 were detected by qRT-PCR.

2.13. Nuclear and cytoplasmic extraction

The PARIS™ Kit (Thermo Fisher Scientific, Waltham, USA) was used for the extraction of nuclear and cytoplasmic fractions in accordance with the manufacturer's instructions. Briefly, the cells were lysed in Cell Fraction Buffer, then, centrifuged at 500 *g* for 3 min. The supernatant was collected as cytoplasmic fraction, and the pellet as nuclear fraction.

2.14. RNA fluorescence in situ hybridization (FISH)

To evaluate circANKHD1, an oligonucleotide modified probe sequence labeled with Biotin for circANKHD1 was obtained from Sangon Biotech (Shanghai, China). The cells were fixed in 4% formaldehyde for 15 min at room temperature and permeabilized in 0.05% Triton X-100 for 10 min at 4 °C. Then, the cells were washed with PBS three times, followed by dehydration with 75%, 80% and absolute ethanol for 5 min. After prehybridization in 2 × SSC at 52 °C for 1 h, hybridization was performed at 37 °C overnight. After rinsing twice in 5 × SSC at 37 °C and washed thrice with 2 × SSC/50% formamide at 37 °C, the samples were incubated with HRP-conjugated streptavidin contained in Alexa Fluor™ 488 Tyramide SuperBoost™ Kits (Thermo Fisher Scientific, Waltham, USA) for 1 h. Then, the samples were stained with DAPI. Finally, the subcellular location of circANKHD1 was detected by a confocal laser scanning microscope.

The sequence of the circANKHD1 specific probe was as follows: 5′-biotin-CCAUCUGAACAAGCUUCUGCUAGACUGCGA-CAUGCAGGCCUCCAUUAAGGCAGUGUGC-3'.

2.15. Mitochondrial membrane potential (ΔΨm) assay

For the detection of mitochondrial membrane potential (ΔΨm), the JC-1 fluorescence with the Mitochondrial Membrane Potential Assay Kit (Invitrogen, Carlsbad, USA) was used in accordance with the manufacturer's instructions. The cells were seeded in 6-well plates at a density of 1×10^5 cells/well, then, incubated with 1 mg/mL JC-1 at 37 °C for 15 min. After washing three times with PBS and covered with 1 μg/mL Hoechst 33342 (Invitrogen, Carlsbad, USA), a Zeiss LSM 800 confocal microscopy was used to detect the fluorescent signals. JC-1 monomers (green) and aggregates (red) fluorescence were observed by excitation at 514 and 585 nm, and emission at 529 and 590 nm, respectively.

2.16. Mitochondrial ROS and cytosolic ROS detection

Mitochondrial ROS and cytosolic ROS were detected by MitoSOX (Invitrogen, Carlsbad, USA) and DCFH-DA (Sigma Aldrich, USA), respectively. The cells were seeded in 6-well plates at a density of 1×10^5 cells/well, and incubated with 5 μM or 10 μM DCFH-DA working solution at 37 °C for 15 min. After washing three times with PBS and covered with 1 μg/mL Hoechst 33342 (Invitrogen, Carlsbad, USA), a Zeiss LSM 800 confocal microscopy was used to detect the fluorescent signals.

2.17. Co-immunoprecipitation, silver staining, and mass spectrometry (MS)

Immunoprecipitation (IP) of LRPPRC, SLIRP, or FLAG was performed using rabbit anti-human LRPPRC antibody (1:100, 21175-1-AP, Proteintech, Chicago, USA) or rabbit anti-human SLIRP antibody (1:100, 26006-1-AP, Proteintech, Chicago, USA) or mouse anti-human FLAG (1:100, 66008-2-Ig, Proteintech, Chicago, USA) at 4 °C for 2 h, followed by incubation with protein A/G magnetic beads (Thermo Fisher Scientific, Waltham, MA, USA) at 4 °C overnight and washing with lysis buffer. Rabbit IgG (1:100, Millipore, USA) was used as the negative control. The purified proteins were resuspended in 1 × SDS sample buffer, heated at 95 °C for 10 min, and subsequently detected by Western blot, silver staining, or MS. The Fast Silver Stain Kit (Beyotime, Haimen, China) was used to perform silver staining in line with the manufacturer's protocol. MS was performed by Wininnovate Bio (Shenzhen, China). Briefly, the purified proteins were extracted with 50% acetonitrile and dried followed by incubation in 10 mM dithiothreitol and 55 mM iodoacetamide. They were then washed with 25 mM ammonium bicarbonate and dried again. After digestion by trypsin at 37 °C overnight, the protein samples were loaded through a 5 μm C18 trap, after 1 h 4%–26% acetonitrile gradient on a C18 column, the samples were analyzed on the Easy nLC 1200 system (Thermo Fisher Scientific, Waltham, USA). The Mascot software (version 2.3.01 Matrix Science, London, UK) was used for analyzing the acquired data, and peak lists were searched against the *Homo sapiens* Uniprot FASTA database.

2.18. Luciferase reporter assay

The sequence of circANKHD1 was cloned downstream of pmirGLO reporter vector (GeneCreate, Wuhan, China). Mutations were created in the binding sites. T24 cells were seeded into 24-well plates at a density of 5×10^3 cells/well for 24 h and then co-transfected with a mixture of 500 ng pmirGLO Dual-Luciferase reporter, 5 ng pRL-CMV Renilla luciferase reporter, and 5 pmol miRNA mimic. After 48 h, the luciferase activity was measured with a dual-luciferase reporter assay system (Promega, Madison, WI).

2.19. Patient-derived UCB organoid assay

Briefly, UCB tumor tissues were minced at about 0.5 cm diameter and disassociated into individual cells via digestion with 5 mg/mL collagenase type II (Life Technologies) with 10 μM Y-27632 dihydrochloride and incubated at 37 °C for 1 h. Then, we filtered the suspension of dissociated cells through a 70 μm mesh filter. The UCB cells were then embedded in Matrigel and cultured with Advanced Dulbecco's modified Eagle's medium/F12 mixed with 500 ng/mL Rspo1, 100 ng/mL Noggin, 50 ng/mL EGF, 10 mM nicotinamide, 500 nM A830-1 (Tocris), 3 mM SB202190 (Sigma), 10 nM prostaglandin E2 (Sigma), penicillin/streptomycin, 10 mM HEPES, 2 mM GlutaMAX, 1 × B27 (Life Technologies),

10 nM gastrin I (Sigma), and 1 mM N-acetylcysteine (Sigma) at 37 °C under 5% CO_2. The medium was obtained from OuMel (Hai Shang, China). For the generation of stable lines, organoids were first digested into individual cells by TrypLE (GIBICO) and incubated with purified lentivirus for 6 h, followed by selection with 2 μg/mL puromycin. For organoids formation assay, the individual organoid cells were seeded onto a 24-well plate with a density of 1000 cells in 50 μL/well. The number and size of the organoids were determined after 2 weeks, and the growth area of organoids was measured and quantified by ImageJ.

2.20. Animal models

All procedures involving mice were approved by the Institutional Animal Care and Use Committee of SYSUCC and were carried out in accordance with the approved guidelines of SYSUCC. Four-week-old Balb/c nude mice were purchased from Charles River Laboratories (Beijing, China). For the xenograft tumor-growth assay, 5×10^6 UCB cells were injected subcutaneously into the four-week-old Balb/c nude mice. Tumor formation in the mice was assessed after 4 weeks.

For the orthotopic xenograft model, the mice were anesthetized by isoflurane (Baxter Healthcare Corporation, Guayama, Puerto Rico, 00784) during the whole surgery process. A 24 G closed IV catheter was inserted into the urethra of mice. After 100 μL hydrochloric acid (0.1 mol/L) injection for about 20 s, 100 μL sodium hydroxide (0.1 mol/L) was infused and retained for the same time. PBS (100 μL) was used to wash the bladder before injecting luciferase-transduced 1×10^6 T24 cells into the bladder, then, the urethra was ligated with suture to maintain the cells for about 30 min. To image the tumors in the bladder, the mice were anesthetized with isoflurane and injected intraperitoneally with 100 μL VivoGloluciferin solution (15 mg/mL; Promega). The orthotopic model observation was subsequently achieved using the IVIS 200 imaging system. Six weeks later, the mice were sacrificed to assess

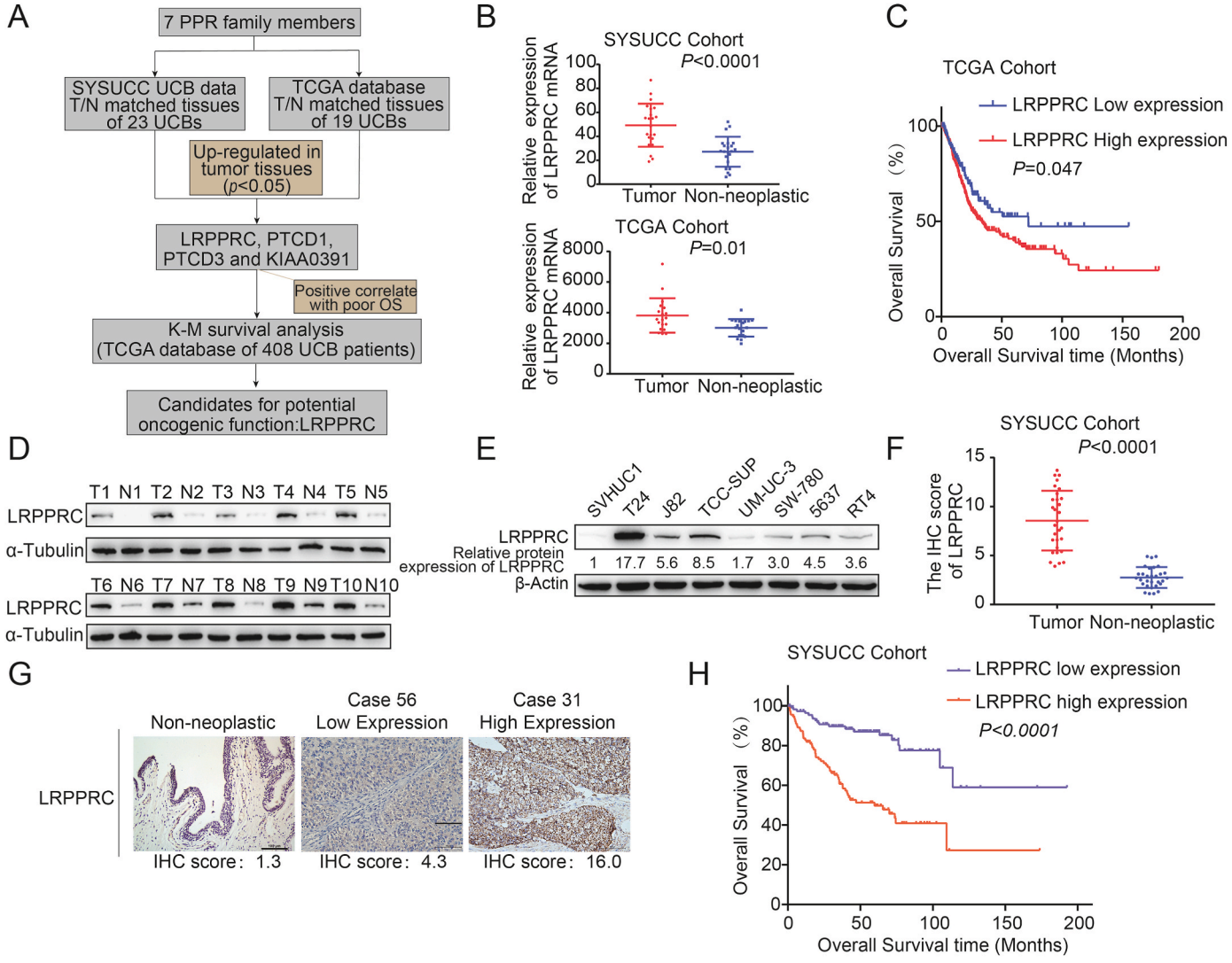

Fig. 1. LRPPRC is overexpressed in UCBs and correlates with patient poor prognosis. (A) Bioinformatics analysis of PPR family members in UCB. LRPPRC was screened as a candidate that had potential oncogenic functions in UCB. N, non-neoplastic bladder tissues; T, tumor tissue. (B) The expression levels of LRPPRC (levels of mRNA expression) in paired UCB tissues and non-neoplastic tissues in the TCGA and SYSUCC cohort. (C) Prognostic significance of LRPPRC in 408 UCB patients (TCGA cohort) assessed by Kaplan–Meier analyses. (D) Western blot analysis of LRPPRC expression in 10 UCB tissues. N, non-neoplastic bladder tissues; T, tumor tissue. Expression of α-Tubulin was used as a loading control. (E) Western blot analysis of LRPPRC expression in 7 human UCB cell lines (ie, T24, J82, TCCSUP, UM-UC-3, SW-870, 5637 and RT4) and a non-tumorigenic cell line, SV-HUC-1. (F) Quantification of immunohistochemical analysis of LRPPRC expression (IHC score) in 30 primary UCBs and matched adjacent non-neoplastic tissues. (G) Representative images of IHC staining of LRPPRC in non-neoplastic bladder tissues and UCB tumor tissues. The normal bladder tissue and one UCB tissue (case 56) had low expression of LRPPRC, whereas another UCB tissue (case 31) had high expression of LRPPRC. The IHC scores were quantified by the HALO image analysis platform. Scale bar, 100 μm. (H) Kaplan-Meier analysis indicating an association between LRPPRC high-expression and poor OS rates in UCB patients (SYSUCC cohort, n = 224 cases).

their bladders.

2.21. Statistical analysis

Statistical analyses were performed using R, GraphPad Prism (version 6.0) or SPSS software (SPSS Standard version 13.0, IBM®, USA). A two-sided chi-square test was used to assess the statistical significance of the association between the expression of LRPPRC and the patient's clinicopathological parameters. Comparisons between groups were performed using the two-tailed Student's *t*-test. OS was assessed using the Kaplan–Meier method and compared by the two-sided log-rank test. The Cox proportional-hazards regression analysis was performed for univariate and multivariate survival analysis. The correlations among LRPPRC, FOXM1, PRDX3 and circANKHD1 expression levels were assessed using the Pearson correlation analysis. P value < 0.05 was considered statistically significant.

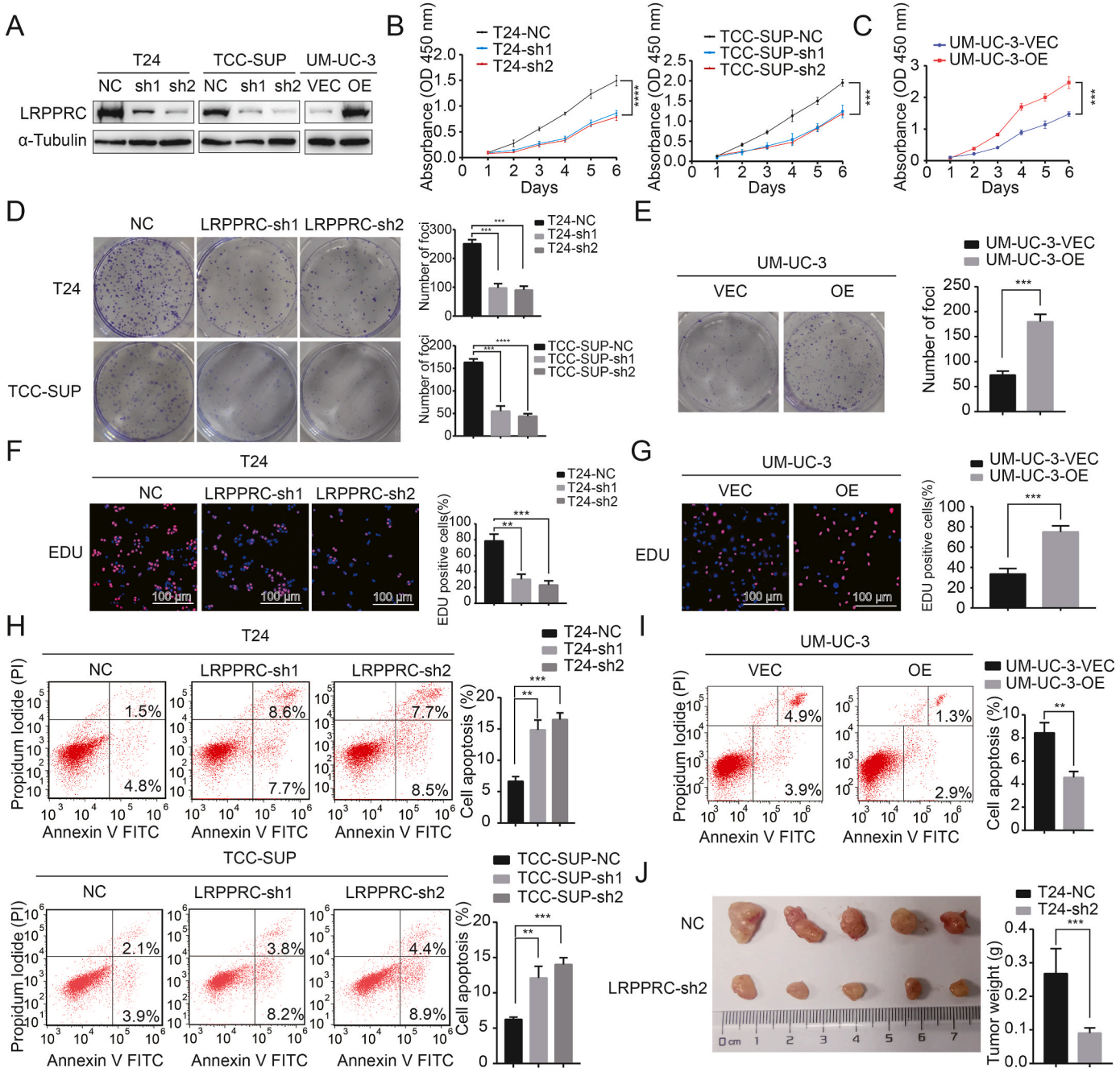

Fig. 2. LRPPRC regulates cell proliferation and apoptosis in UCB cells. (A) Western blotting reveals that LRPPRC was efficiently knocked down and overexpressed in corresponding cells. (B-C) CCK-8 assays of the cell growth ability of the indicated UCB cells. (D–E) Colony formation assays of the indicated UCB cells. Columns: mean ± standard deviation (SD) of three independent experiments. (F–G) EDU assays of the indicated UCB cells. Columns: mean ± standard deviation (SD) of three independent experiments. (H-I) Apoptosis of UCB cells with modulation of LRPPRC expression was detected by flow cytometric analysis as indicated. Columns: mean ± standard deviation (SD) of three independent experiments. (J) Down expression of LRPPRC in the T24 cell line substantially repressed tumor formation compared with T24-NC cells. Left, images of the xenograft tumors formed in Balb/c nude mice injected with T24-NC or T24-shLRPPRC cells. Right, weights of xenograft tumors (n = 5). $^{**}P < 0.01$; $^{***}P < 0.001$; $^{****}P < 0.0001$.

3. Results

3.1. Increased expression of LRPPRC correlates with poor survival of UCB patients

To investigate the dynamics of PPR alteration in UCB, we performed bioinformatics analysis in the cohort of UCBs from the SYSUCC (GSE133671) and TCGA databases (Fig. 1A). We found that LRPPRC, PTCD1, PTCD3, and KIAA0391 were overexpressed in UCB tissues compared with matched non-neoplastic bladder tissues (Fig. 1B, Supplementary Figs. 1A–B). Further, Kaplan–Meier analyses demonstrated that high expression levels of LRPPRC were associated with poor OS in the 408 UCB patients from the TCGA cohort (Fig. 1C, Supplementary Fig. 1C). Therefore, we focused on exploring the potential clinical significance and biological functions of LRPPRC in UCBs. Western blot assay was performed in 10 pairs of primary UCB and adjacent non-neoplastic bladder tissues. The results showed that LRPPRC was frequently upregulated in UCB tissues compared with adjacent non-neoplastic bladder tissues (Fig. 1D). In addition, compared with normal uroepithelium cell line SV-HUC-1, the expression of LRPPRC was clearly upregulated in seven UCB cell lines (Fig. 1E).

To further investigate the potential clinical significance of LRPPRC expression in UCB patients, we examined the protein expression of LRPPRC by IHC in 224 primary UCB samples, among which there were 30 samples with paired adjacent non-neoplastic bladder tissue. We found that LRPPRC was significantly upregulated in 30 UCB tissue samples compared with adjacent normal bladder tissue samples (Fig. 1F). The representative IHC staining of LRPPRC in UCB tissue and non-neoplastic bladder tissue is shown in Fig. 2G. Correlation analysis demonstrated that a high expression of LRPPRC was closely associated with larger tumor size ($P < 0.001$; Supplementary Table 1), higher T stage ($P < 0.001$; Supplementary Table 1) and higher N stage ($P < 0.001$; Supplementary Table 1). In univariate analysis (Supplementary Table 2), several well-established prognostic parameters had a significant effect on patient OS, including tumor size ($P = 0.030$), pT stage ($P < 0.001$), pN stage ($P < 0.001$) and tumor grade ($P = 0.014$). Importantly, Kaplan–Meier survival analysis validated that high expression of LRPPRC was significantly associated with poorer OS in UCB patients (Fig. 1H; $P < 0.001$; Supplementary Table 2). Multivariate analysis showed that high expression of LRPPRC was an independent prognostic factor in UCB (hazard ratio [HR]: 2.292, confidence interval [CI]: 1.225–4.290, $P = 0.009$; Supplementary Table 2).

3.2. LRPPRC regulates cell proliferation and apoptosis in UCB cells in vitro and in vivo

Considering that LRPPRC was upregulated in UCB and high expression levels of LRPPRC were related to the larger tumor size and poor prognosis of the patients, we further evaluated the effect of LRPPRC on proliferation and apoptosis in UCB cells. To investigate the impact of perturbing LRPPRC expression in UCB cells, LRPPRC was knocked down in T24 and TCC-SUP cells (high LRPPRC expression) and overexpressed in UM-UC-3 cells (low LRPPRC expression) using two shRNAs and an overexpression plasmid of LRPPRC (Fig. 2A). We found that knockdown of LRPPRC in UCB cells dramatically decreased cell growth (Fig. 2B), colony formation (Fig. 2D), and EDU-positive cells (Fig. 2F) and increased cell apoptosis (Fig. 2H). In contrast, ectopic overexpression of LRPPRC significantly increased cell growth (Fig. 2C), colony formation (Fig. 2E) and EDU-positive cells (Fig. 2G), and decreased cell apoptosis (Fig. 2I).

Next, we used a subcutaneous xenograft tumor mouse model to validate the biological functions of LRPPRC *in vivo*. We observed that knockdown of LRPPRC in UCB cells substantially reduced the abilities of subcutaneous tumor formation (Fig. 2J). Taken together, our results reveal that LRPPRC may play a critical role in the proliferation and apoptosis of UCB cells, both *in vitro* and *in vivo*.

3.3. LRPPRC regulates the expression of mitochondrial mRNAs and FOXM1 in UCB cells

To further explore the mechanism of LRPPRC in UCB cells' proliferation and apoptosis, RNA sequencing was used to compare the global gene expression profiles of T24 cells transfected with LRPPRC-sh2 and non-targeting control shRNA (sh-NC). The DEGs are shown in Fig. 3A. Specifically, 888 genes were downregulated and 912 were upregulated in LRPPRC-sh2 T24 cells (Fig. 3A, Supplementary Data 2). Then, we used the genes with $|\log2(\text{fold change})|>1$ for KEGG and GO pathway analysis. The results showed that LRPPRC was closely related to cell apoptosis signaling pathway (Fig. 3B, $P < 0.01$), which was consistent with the results of the functional experiments in UCB cells. We also found that LRPPRC was positively associated with the oxidative phosphorylation (OXPHOS) signaling pathway (Fig. 3B, $P < 0.01$). In addition, GO analysis showed that LRPPRC was associated with the electron transport chain (ETC) in T24 cells (Fig. 3C).

Mitochondrial metabolism, including OXPHOS, is critical for tumorigenesis by orchestrating cellular apoptosis, ROS production and energy transformation [31,32]. Among 888 genes downregulated in LRPPRC-sh2 T24 cells, 12 mRNAs encoded by mitochondrial (mtRNAs, mt-CO1, mt-CO2, mt-CO3, mt-CYB, mt-ND1, mt-ND2, mt-ND3, mt-ND4, mt-ND4L, mt-ND6, mt-ATP6, and mt-ATP8) were downregulated (Fig. 3D). This result was further verified by qRT-PCR, which showed that the knockdown of LRPPRC significantly downregulated the expression levels of these 12 mt-mRNAs (Fig. 3E). Moreover, FOXM1, which is closely related to cell ROS metabolism, proliferation and apoptosis, was also downregulated in LRPPRC-sh2 T24 cells (Fig. 3D). Given that FOXM1 and PRDX3 (the downstream of FOXM1) play critical roles in the regulation of oxidative stress during oncogenesis [33], we further analyzed the correlation between the expression levels of LRPPRC and FOXM1 and/or PRDX3 in the UCB cohort derived from the TCGA UCB database. As anticipated, the results showed a significantly positive correlation between LRPPRC and FOXM1 ($r = 0.2720$, $P < 0.0001$, Fig. 3F) and/or PRDX3 ($r = 0.3426$, $P < 0.0001$, Fig. 3F). Western blot analysis further showed that knockdown of LRPPRC downregulated FOXM1 and its downstream ROS scavenger genes (PRDX3, MnSOD, and Catalase), while overexpression of LRPPRC upregulated these proteins in UCB cells (Fig. 3G).

3.4. LRPPRC regulates apoptosis via oxidative stress in UCB cells

Given that the ETC plays an important role in OXPHOS activity and that 13 proteins encoded by mt-mRNAs are involved in the organization of the ETC complex, proton pumps of the ETC generate mitochondrial membrane potential ($\Delta\Psi m$). Therefore, we detected $\Delta\Psi m$ by JC-1 fluorescence in T24-NC and T24-shLRPPRC cells and found that $\Delta\Psi m$ in LRPPRC knockdown cells was markedly lower as compared to T24-NC cells (Fig. 3H). Considering that the $\Delta\Psi m$ decrease indicates mitochondrial stress, and ROS often increases mitochondrial stress [34]; besides, FOXM1, the potential downstream of LRPPRC, has been reported to regulate intracellular ROS levels to protect cancer cells from oxidative stress [33,35], we hypothesized that LRPPRC might play an important role in UCB cells' ROS metabolism. Thus, we evaluated both mitochondrial ROS (mROS) and cytosolic ROS (cROS) through fluorescent dyes MitoSOX and DCFH-DA. In parallel to $\Delta\Psi m$ decrease, both mROS and cROS were significantly increased in LRPPRC knockdown cells (Fig. 3H). These data indicate that LRPPRC affects oxidative stress in UCB cells through both the production and elimination of mROS and cROS.

It is known that ROS can serve as signaling molecules to promote cell growth at low or moderate levels but high levels of ROS can induce cell apoptosis [36]. Our results showed that knockdown of LRPPRC elevated intracellular amounts of ROS, which were sufficient to trigger cell apoptosis. Thus, we performed Western blot analysis to identify the role of LRPPRC in the UCB apoptotic pathway. Our results showed that the

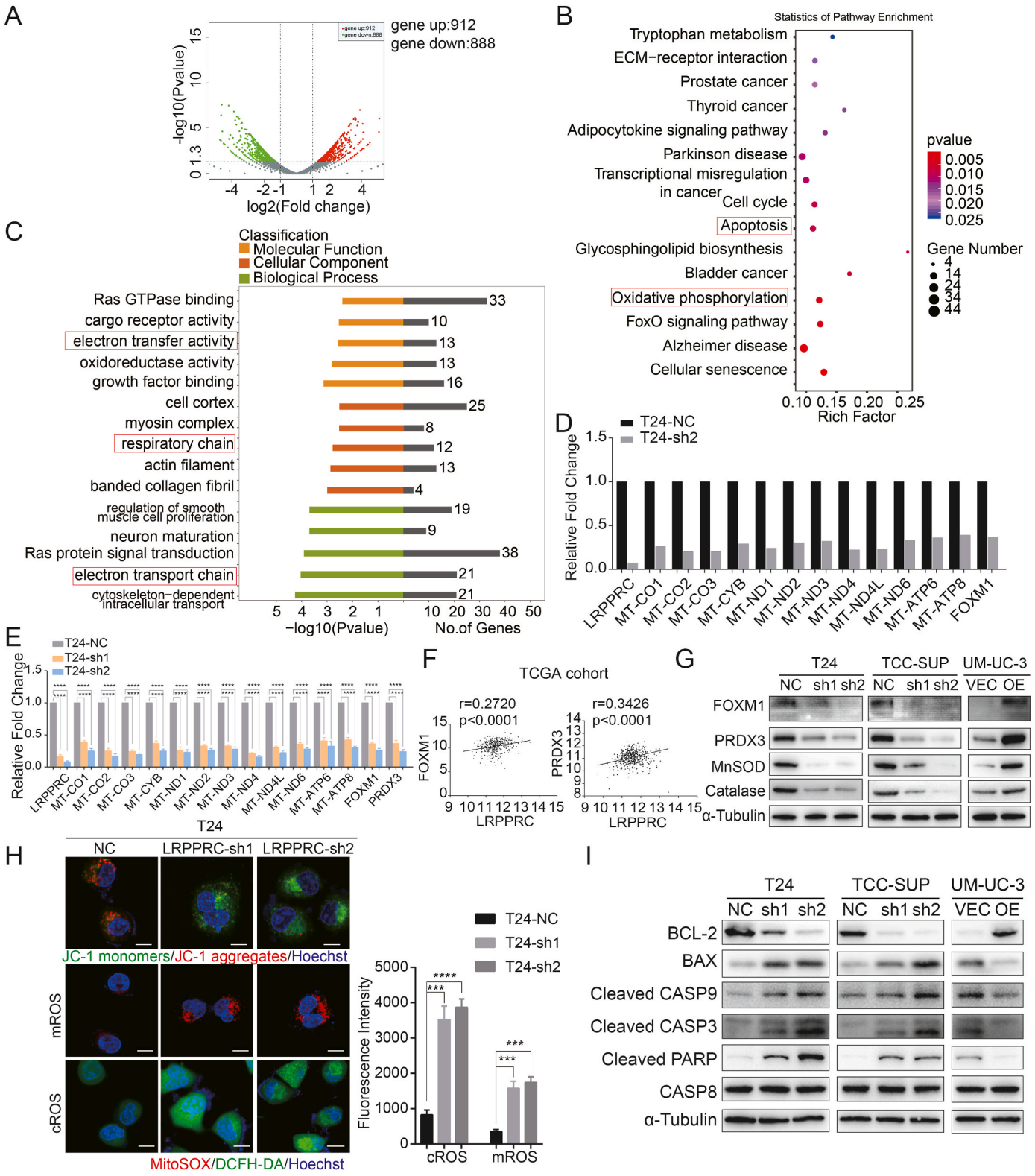

(caption on next page)

Fig. 3. LRPPRC regulates apoptosis and oxidative stress in UCB cells. (A) Volcano plot comparing the global gene expression profiles of T24 cells transfected with LRPPRC-sh2 and sh-NC. (B) GSEA analysis showing LRPPRC-related KEGG pathways in T24 cells (T24-NC vs T24-shLRPPRC). (C) GO analysis was performed using genes with |log2(fold change)|>1 by comparing T24-NC with T24-shLRPPRC. The five most involved GO terms are displayed. (D) 12 mRNAs encoded by mitochondrial (mtRNAs, mt-CO1,mt-CO2,mt-CO3,mt-CYB, mt-ND1,mt-ND2, mt-ND3, mt-ND4, mt-ND4L, mt-ND6, mt-ATP6, and mt-ATP8) and FOXM1 were downregulated in T24-shLRPPRC cells compared with T24-NC cells. (E) The expression of 12 mt-mRNAs, FOXM1 and PRDX3 in T24-shLRPPRC cells were assessed by qRT-PCR and presented as fold change relative to T24-NC cells. Columns: mean ± standard deviation (SD) of three independent experiments, $^{****}P < 0.0001$. (F) LRPPRC expression was positively correlated with the expression of FOXM1 (left) and PRDX3 (right) in UCB patients derived from the TCGA database. (G) Western blots comparing LRPPRC-silenced and LRPPRC-overexpressing UCB cells with their respective control cells are shown for relative expression of FOXM1, PRDX3, MnSOD and Catalase. α-Tubulin expression was used as a loading control. (H) ΔΨm of T24-NC and T24-shLRPPRC was assessed by JC-1 staining (Top). JC-1 monomers (green) and aggregates (red) were detected by confocal microscopy. Scale bar, 10 μm. Mitochondrial ROS (mROS) and cytosolic ROS (cROS) were detected using fluorescent dyes of MitoSOX and DCFH-DA (Bottom). Scale bar, 10 μm. Fluorescence intensity was analyzed by Image J. Columns: mean ± standard deviation (SD) of three independent experiments, $^{***}P < 0.001$. (I) Western blots comparing LRPPRC-silenced and LRPPRC-overexpressing UCB cells with their respective control cells for relative expression of BCL-2, BAX, cleaved-caspase3, cleaved-caspase9, cleaved-PARP and caspase8. α-Tubulin expression was used as a loading control. (For interpretation of the references to colour in this figure legend, the reader is referred to the Web version of this article.)

expression levels of the intrinsic apoptosis markers, such as cleaved-caspase3, cleaved-caspase9 and cleaved-PARP, were upregulated after LRPPRC knockdown and downregulated after LRPPRC overexpression (Fig. 3I). Furthermore, the expression of BCL-2 protein was downregulated (upregulated) while that of BAX protein was upregulated (downregulated) after LRPPRC knockdown (overexpression) (Fig. 3I). However, the level of caspase8, an extrinsic apoptosis marker, did not change significantly (Fig. 3I). These results imply that LRPPRC inhibits UCB cell caspase-dependent apoptosis via the stabilization of the mitochondrial membrane potential and the levels of mROS and cROS.

3.5. SLIRP forms a complex with LRPPRC to enhance its stability and to prevent LRPPRC from degradation

The LRPPRC protein could be degraded by mitochondrial matrix protease such as lon peptidase 1 (LONP1), with a half-life of around 20 h in LUAD cells [37,38]. To identify the potential binding partners of LRPPRC, the whole-cell protein lysates from UM-UC-3 and T24 cells were used for IP with IgG and a specific LRPPRC antibody. The differential protein bands in the resultant immunoprecipitate were detected by silver staining (Fig. 4A). In order to identify the differential protein bands, both the resultant immunoprecipitates of T24-IgG and T24-LRPPRC were analyzed by MS (Fig. 4B, Supplementary Data 3). We found that SLIRP was one of the major binding partners of LRPPRC (Fig. 4A and B, Supplementary Table 3). The interaction between LRPPRC and SLIRP was further confirmed through co-IP in T24 cells (Fig. 4B). Moreover, immunofluorescent staining was conducted to validate the co-localization between LRPPRC and SLIRP (Fig. 4C).

Previous studies have shown the interaction between LRPPRC and SLIRP [19,39], but little is known about the complex in UCB cells. In this study, Western blot was used to reveal the regulatory relationship between LRPPRC and SLIRP. The results showed that the level of SLIRP was repressed when LRPPRC was knocked down, while SLIRP was elevated when LRPPRC was overexpressed (Fig. 4D). Moreover, the overexpression of SLIRP was able to rescue the protein level of LRPPRC in T24-shLRPPRC cells, while knockdown of SLIRP downregulated the protein level of LRPPRC in UM-UC-3 OE-LRPPRC cells (Fig. 4D). These results are consistent with previous research that LRPPRC and SLIRP are mutually interdependent [19,21,39]. As recently reported, SLIRP enhances the stability of LRPPRC by preventing the aggregation and/or degradation of LRPPRC [37,39] but little is known about the regulation of this mechanism in UCB cells. We wondered whether SLIRP stabilized LRPPRC through inhibition of the ubiquitin-proteasome pathway in UCB cells. Thus, to assess the role of proteasome in LRPPRC degradation, T24 cells were transfected with si-NC or si-SLIRP and treated with the proteasome inhibitor, MG132. We showed that LRPPRC was upregulated in both T24-NC and T24-siSLIRP cells after treatment with MG132 (Fig. 4E). In addition, the expression levels of LRPPRC decreased more significantly after the knockdown of SLIRP in T24 cells treated with CHX (Fig. 4F). Moreover, we performed ubiquitination assay by co-transfecting T24 cells with Flag-LRPPRC and HA-ubiquitin in the si-NC or si-SLIRP cells. Our findings further validated that the downregulation of SLIRP significantly increased the amount of poly-ubiquitinated LRPPRC (Fig. 4G). These data offer evidence that SLIRP forms a complex with LRPPRC to enhance its stability and to prevent LRPPRC from ubiquitination and proteasomal degradation in UCBs. Moreover, the suppressed proliferation of LRPPRC-silenced T24 cells was rescued by the overexpression of SLIRP, which indicates that LRPPRC and SLIRP may promote the growth of UCB cells as a complex (Fig. 4H).

3.6. circ-ANKHD1 is screened as the downstream target regulated by LRPPRC

It is well known that LRPPRC is involved in mRNA stability, so it would be interesting to determine whether small RNAs such as circle RNAs (circRNAs) and miRNAs are regulated by LRPPRC [25]. Since there has been no evidence to support that LRPPRC stabilizes the mRNA of FOXM1, we wondered whether LRPPRC-induced FOXM1 upregulation occurred through the regulation of small ncRNAs. Therefore, circRNA sequencing was used to compare the global circRNA expression profiles of T24 cells transfected with LRPPRC-sh2 and sh-NC. The differentially expressed circRNAs are shown in Fig. 5A. Of them, 39 circRNAs were downregulated and 31 were upregulated in LRPPRC-sh2 T24 cells (Supplementary Data 4).

Next, we examined the top three downregulated/upregulated circRNAs by qRT-PCR. The results showed that the expression of circANKHD1 (hsa_circ_0001541), but not that of the other five circRNAs, changed significantly after silencing LRPPRC (Supplementary Fig. 2A). CircANKHD1 is located on chromosome 5:139819703–139828890 and it consists of exon 4–7 of ANKHD1 (Fig. 5D). We further demonstrated that the levels of circANKHD1 were decreased in both LRPPRC-silenced UCB cell lines and increased in LRPPRC-overexpression cell line (Fig. 5B). We further examined the 5' neighboring genes of ANKHD1 and found that knockdown of circANKHD1 or overexpression of circANKHD1 had no effect on the neighboring genes (Supplementary Figs. 2B–C).

Further, we aimed to characterize circANKHD1 in UCB cells. The expression level of circANKHD1 was detected in a normal uroepithelium cell line SV-HUC-1 and in seven UCB cell lines. The results showed that the expression level of circANKHD1 was upregulated in UCB cells and positively correlated with the expression of LRPPRC in UCB cells (Fig. 5C). Furthermore, circANKHD1 was analyzed by RT-PCR and Sanger sequencing (Fig. 5D). The sequenced PCR product of divergent primers was corresponding from the 5′ exon7 to 3' exon4 (Fig. 5D). In addition, RNaseR or actinomycin D treatment assay showed that circANKHD1 was resistant to RNaseR and was more stable than the linear mRNA of ANKHD1 (Fig. 5D–F). The examination of mRNA fractionation and FISH validated the predominant cytosolic distribution of circANKHD1 in T24 cells (Fig. 5G and H).

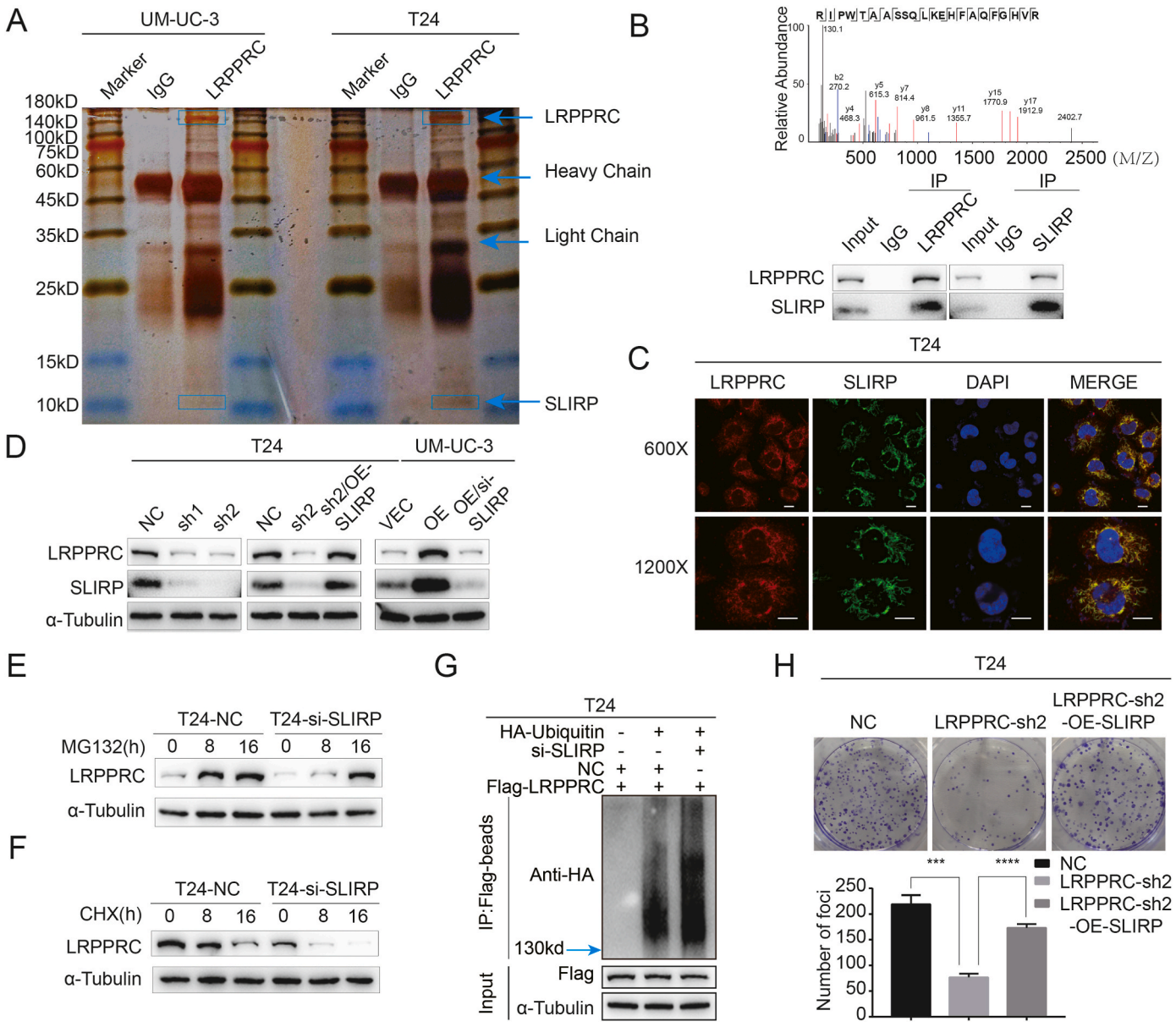

Fig. 4. SLIRP forms a complex with LRPPRC to enhance its stability and to prevent LRPPRC from degradation. (A) LRPPRC interaction partners were detected in UM-UC-3 and T24 cells. Silver staining is used for the detection of differential protein bands. The band of LRPPRC and SLIRP are indicated by arrows. (B) Mass spectrometry identified SLIRP, which was pulled down from T24 cell lysates by LRPPRC (Top). The interaction between LRPPRC and SLIRP was confirmed by co-immunoprecipitation in T24 cells (Bottom). (C) Confocal staining presented the co-localization of LRPPRC and SLIRP in T24 cells. (D) Western blots revealed the regulatory relationship between LRPPRC and SLIRP. (E) siNC and siSLIRP were transfected in T24 cells, and 48 h later, the cells were treated with 10 μM of MG132 for various number of times and the cell lysates were immunoblotted as indicated. (F) T24-NC and T24-siSLIRP cells were treated with 50 μg/mL cycloheximide. Whole-cell lysates were harvested at the indicated times and the cell lysates were immunoblotted as indicated. (G) Flag-LRPPRC and HA-ubiquitin were transfected to T24-NC and T24-siSLIRP cells. The cells were treated with 10 μM MG132 for 8 h before harvest. Cell lysates were immunoprecipitated with Flag antibody and immunoblotted as indicated. (H) Colony formation assays show that knockdown of LRPPRC inhibited UCB cell proliferation capacity which was reversed by SLIRP overexpression. Error bars: mean ± SD of three independent experiments. ***$P < 0.001$; ****$P < 0.0001$.

3.7. Upregulation of circANKHD1, induced by LRPPRC, regulates the expression levels of FOXM1 by reducing the inhibitory effect of miR-671-5p and miR-507 via sponge activity

Given that miRNA sponge is one of the most crucial mechanisms of circRNA [40] and that circANKHD1 is stable and abundant in the cytoplasm, we examined whether circANKHD1 regulated FOXM1 through the sponge mechanism. Using the TargetScan miRNA prediction program [41], 26 miRNAs were found to contain at least one binding site for the circANKHD1 region (Supplementary Data 5). Then, TarPmiR and TargetScan were used to find miRNAs that could directly target the 3′UTR of FOXM1. A total of 2001 and 450 miRNAs were predicted by TarPmiR and TargetScan, respectively, as potential factors that may regulate the expression of FOXM1 [41,42] (Supplementary Data 6). After merging this cluster of miRNAs, we screened out only two miRNAs that might be related to circANKHD1 and FOXM1 (Fig. 5I, Supplementary Fig. 2D). To determine whether these two miRNAs could bind to circANKHD1, we further constructed a circANKHD1 fragment and inserted it downstream of the luciferase gene. The results showed that both miR-671-5p and miR-507 mimics significantly reduced the luciferase reporter activity (Fig. 5J). Moreover, we observed that after mutating the miR-671-5p and miR-507 target sites from the luciferase

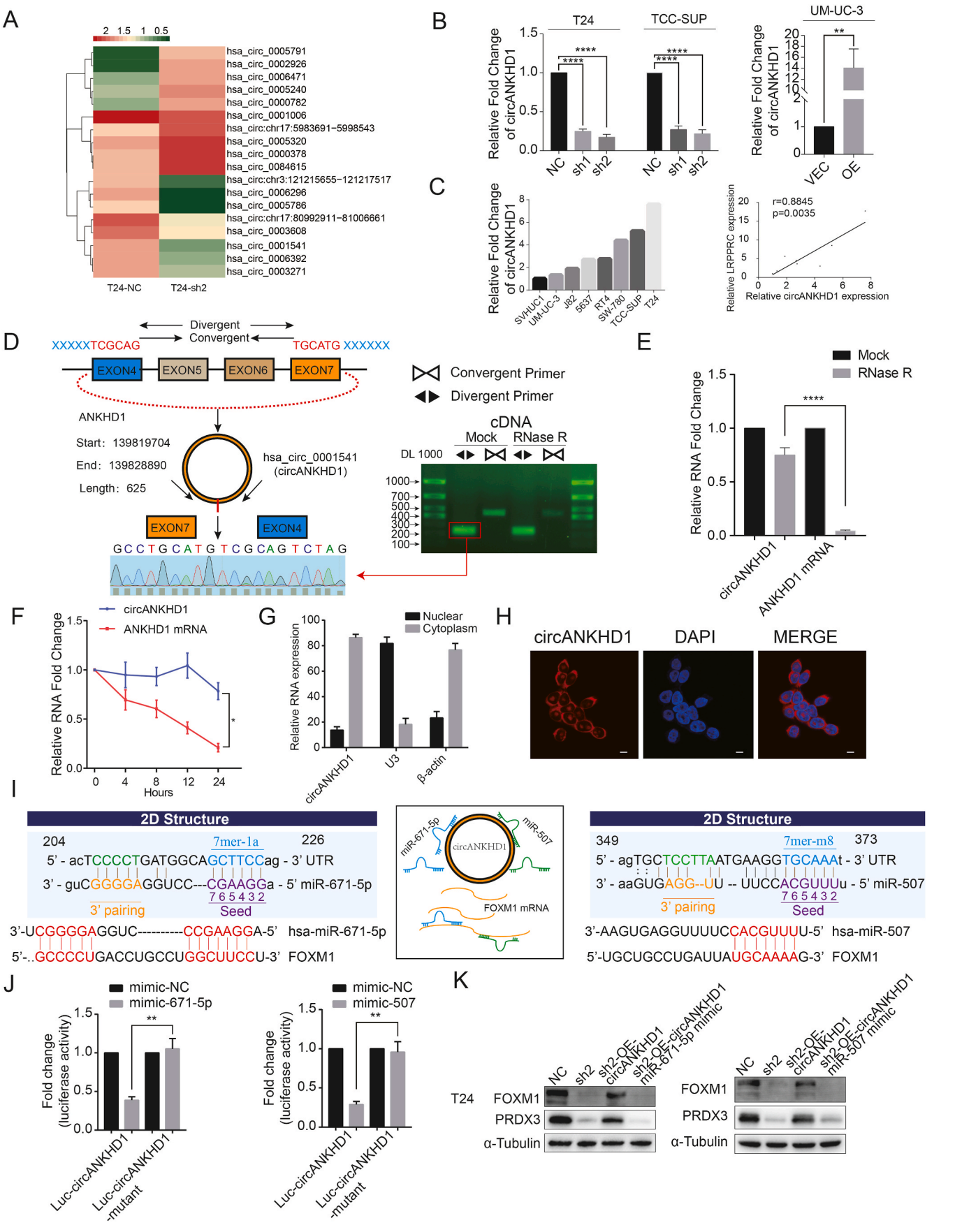

(caption on next page)

Fig. 5. LRPPRC-induced upregulation of circANKHD1 regulates the expression of FOXM1 by reducing the inhibitory effect of miR-671-5p and miR-507 via sponge activity. (A) Clustered heatmap for the circRNA expression profiles of T24 cells transfected with LRPPRC-sh2 and sh-NC. The circRNAs are classified according to Pearson correlation analysis. The numerical data represent the serial number of circRNAs in circBase. (B) qRT-PCR for circANKHD1 in UCB cells treated with two LRPPRC shRNAs (Left). qRT-PCR for circANKHD1 in UCB cells transfected with control vector or LRPPRC overexpression plasmid (Right). Data are presented as fold change relative to T24-NC, TCC-SUP-NC or UM-UC-3-Vec cells ±SD of three experiments, $^{**}P < 0.01$. (C) qRT-PCR for the abundance of circANKHD1 in UCB cells, compared with a non-tumorigenic cell, SV-HUC-1 (Left). Data are presented as fold change relative to SV-HUC-1. LRPPRC is positively associated with circANKHD1 in UCB cells (Right). (D) Verification that circANKHD1 is a circRNA, using divergent and convergent primers. Left, schematic illustration of circANKHD1 locus with specific primers. RT-PCR products with divergent primers showing circularization of circANKHD1. Right, Sanger sequencing to confirm the specific back splicing site of circANKHD1. (E) qRT-PCR for the abundance of circANKHD1 and ANKHD1 mRNA with the treatment of Rnase R in T24 cells. Data are presented as fold change relative to Mock T24 cells ±SD of three experiments, $^{****}P < 0.0001$. (F) qRT-PCR for the half-life analysis of circANKHD1 and ANKHD1 mRNAs with the treatment of actinomycin-D in T24 cells. Data are presented as fold change relative to the mRNA expression level at the time point of 0-h ± SD of three experiments, $^{*}P < 0.05$. (G) Cytoplasmic and nuclear mRNA Fractionation experiment showing that circANKHD1 is mainly located in the cytoplasm. β-actin and U3 were applied as positive controls in the cytoplasm and nucleus, respectively. Data shown are the means ± SD of three experiments. (H) RNA fluorescence *in situ* hybridization for circANKHD1. Nuclei were stained with DAPI. Scale bar, 10 μm. (I) A schematic drawing showing the putative binding sites of the miRNAs associated with circANKHD1 and FOXM1. (J) Luciferase reporter assay for the luciferase activity of LUC-circANKHD1 or LUC-circANKHD1-mutant in T24 cells co-transfected with miRNA mimics. Data shown are the means ± SD of three experiments. $^{**}P < 0.01$. (K) The expression levels of FOXM1 and PRDX3 were enhanced bycircANKHD1 overexpression but were inhibited by miR-671-5p or miR-507 mimics as observed in WB.

reporter with circANKHD1 in the 3′UTR, the miRNA mimics had no significant effect on luciferase activity (Fig. 5J). Further Western blot assay showed that the downregulation of FOXM1 induced by the silencing of LRPPRC could be rescued by the overexpression of circANKHD1, and meanwhile, the level of PRDX3, a well-known downstream of FOXM1 [33,35], was substantially rescued (Fig. 5K). In addition, the increased FOXM1 and PRDX3 levels were largely prevented after treatment with miR-671-5p and/or miR-507 mimics in shLRPPRC-OE-circANKHD1 UCB cells (Fig. 5K). These results, collectively, reveal that LRPPRC-induced upregulation of circANKHD1 regulates the expression of FOXM1 by reducing the inhibitory effect of miR-671-5p and miR-507 by sponge activity.

3.8. LRPPRC promotes cell growth of UCB is partially dependent on circANKHD1

To investigate whether or not LRPPRC exerts its oncogenic effect through the circANKHD1/FOXM1 axis, ectopic circANKHD1 was transfected to UCB cells on an LRPPRC knockdown background in which the circANKHD1 level was downregulated. This model was used to validate whether LRPPRC depletion could be rescued by circANKHD1. qRT-PCR analysis showed that the expression levels of circANKHD1 and FOXM1 were repressed by the knockdown of LRPPRC, and were increased after transfection with ectopic circANKHD1 plasmid (Fig. 6A). Western blot assay showed that the reduction of FOXM1, accompanied by its downstream ROS scavenger genes, PRDX3, MnSOD and Catalase, was largely reversed after the overexpression of circANKHD1 (Fig. 6A). The JC-1 fluorescence revealed that, after the overexpression of circANKHD1, the suppression of ΔΨm in LRPPRC-silenced T24 cells was rescued (Fig. 6B). Meanwhile, the overexpression of circANKHD1 reduced both mROS and cROS levels in LRPPRC-silenced T24 cells (Fig. 6B). Moreover, the suppressed proliferation of LRPPRC-silenced T24 cells was rescued by the overexpression of circANKHD1 (Fig. 6C). Similarly, the overexpression of circANKHD1 reversed the increased apoptosis resulting from LRPPRC knockdown (Fig. 6D). In addition, the overexpression of circANKHD1 reversed the upregulated expression of the intrinsic apoptosis markers, such as cleaved-caspase3, cleaved-caspase9, cleaved-PARP and BAX, and the downregulated expression of BCL-2, without affecting the expression level of caspase8 (Fig. 6E).

To further assess whether circANKHD1 contributed to LRPPRC effects in UCB tumorigenesis, we performed organoid assays using LRPPRC-NC and LRPPRC-silenced background. qRT-PCR and Western blot assays validated that the LRPPRC-knockdown-induced downregulation of FOXM1 was rescued after the overexpression of circANKHD1 in LRPPRC-silenced organoid UCB cells (Fig. 6F). The suppressed proliferation of LRPPRC-silenced organoids was rescued by the overexpression of circANKHD1 (Fig. 6F). Our *in vivo* orthotopic xenograft bladder model in Balb/c nude mice studies also supported the view that the oncogenic role of LRPPRC in UCB cells' growth was dependent on the circANKHD1, at least partially. The mouse bladders implanted with LRPPRC-deleted T24 cells showed small lesions in contrast to the larger tumor lesions that were observed in the bladders embedded with T24-NC cells (Fig. 6G). Further, this inhibitory effect on UCB cell growth induced by LRPPRC deletion could be restored by the overexpression of circANKHD1 (Fig. 6G).

3.9. LRPPRC regulates the circANKHD1/FOXM1 axis to promote UCB tumorigenesis

Given the crucial role of the LRPPRC/SLIRP complex in the regulation of the circANKHD1/FOXM1 axis in UCB tumorigenesis, we further analyzed the clinical significance of the LRPPRC/circANKHD1/FOXM1/PRDX3 pathway in orthotopic xenograft bladder model and patients with UCB. We found that the expression levels of FOXM1 and PRDX3 decreased after the knockdown of LRPPRC, and were restored by the overexpression of circANKHD1 (Fig. 7A–B). The levels of LRPPRC positively correlated with circANKHD1 and FOXM1 expression levels, and the levels of circANKHD1 positively correlated with those of FOXM1 in UCB cases from the SYSUCC cohort (Fig. 7C and D). Taken together, these data suggest the potential oncogenic role of the LRPPRC/circANKHD1/FOXM1 pathway in UCBs.

4. Discussion

Mitochondria are integral in tumorigenesis given that multiple aspects of mitochondrial functions, including metabolism, oxidative stress regulation, cell death susceptibility and signaling, are involved in tumorigenesis [9,43]. Accumulating evidence indicates that PPR proteins can play an important role in mitochondria [12]. Nevertheless, the biological function and molecular mechanisms of PPR proteins in UCB tumorigenesis are largely unknown. In the present study, bioinformatics analysis of RNA-seq data from the SYSUCC and TCGA cohorts showed that LRPPRC was overexpressed in UCBs and was positively associated with larger tumor size, advanced clinical stage, and/or poor clinical prognosis. These findings suggested LRPPRC as a potential prognostic factor in UCB.

Recent studies have also reported that the expression of LRPPRC is upregulated in multiple tumor types, including lung adenocarcinoma [26], esophageal squamous cell carcinoma, gastric cancer, colon cancer, mammary and endometrial adenocarcinoma, lymphoma, and prostate cancer [44–49], which are consistent with our findings. According to Zhang et al. [49], LRPPRC is a potential oncogene in prostate cancer, in which LRPPRC level is negatively associated with biochemical progression-free and overall survival. Therefore, we hypothesized that LRPPRC might play an important role in the development and/or progression of UCB. Thus, a series of *in vitro* and *in vivo* experiments in UCB

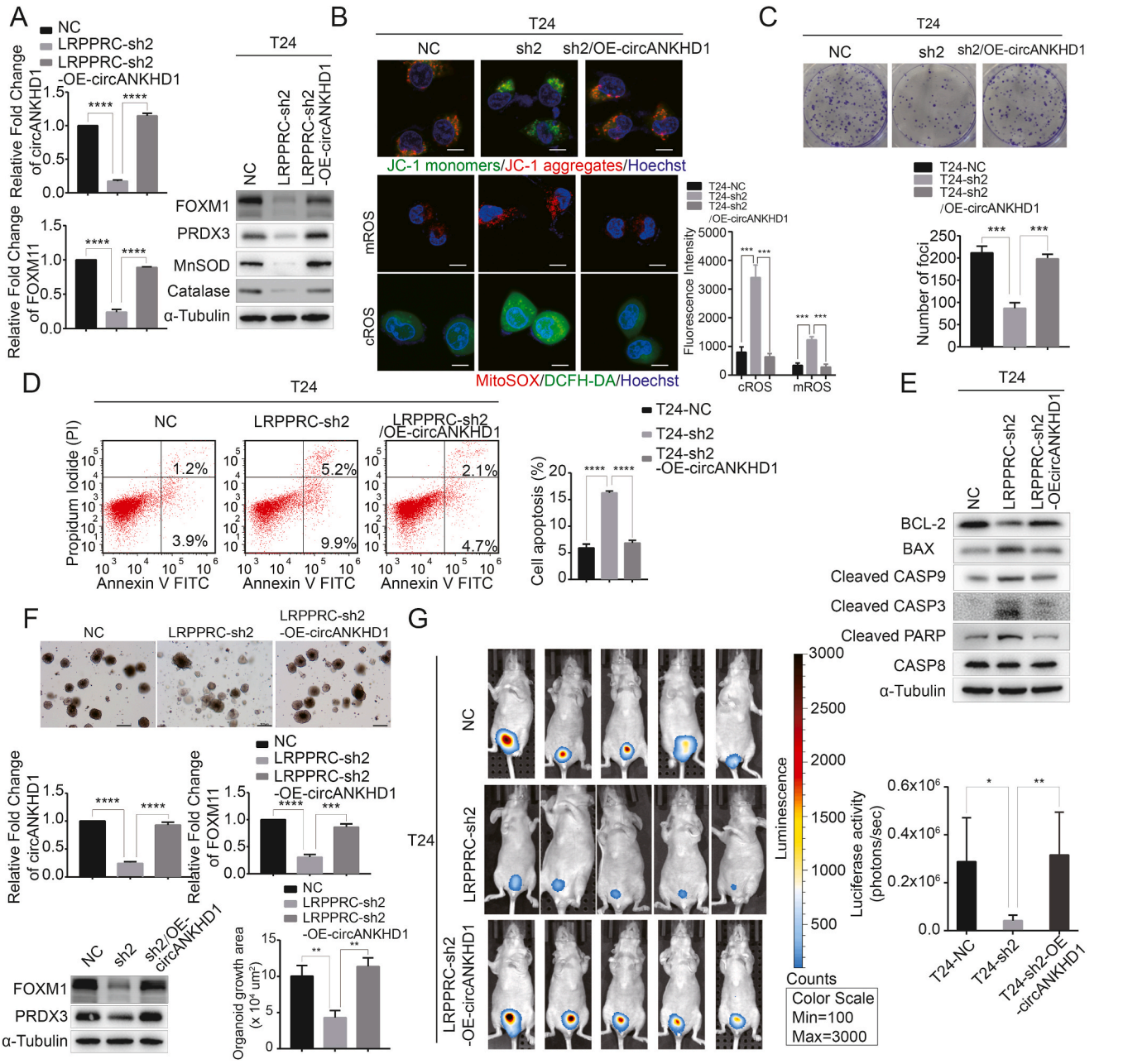

Fig. 6. LRPPRC promotes proliferation and attendances apoptosis is partially dependent on circANKHD1 in UCB cells. (A) qRT-PCR analysis verified that the expression of circANKHD1 and FOXM1, were repressed by the knockdown of LRPPRC and was greatly increased after transfected with ectopic circANKHD1 plasmid (Left). Data shown are presented as fold change relative to T24-NC cells ±SD of three experiments,$^{**}P < 0.01$,$^{***}P < 0.001$, $^{****}P < 0.0001$. Western blot assay showed that the reduction of FOXM1, PRDX3, MnSOD and Catalase, were largely reversed after the overexpression of circANKHD1 (Right). (B) ΔΨm of T24-NC, T24-shLRPPRC and T24-shLRPPRC-OE-circANKHD1 was assessed by JC-1 staining. JC-1 monomers (green) and aggregates (red) were detected by confocal microscopy. Scale bar, 10 μm. Mitochondrial ROS (mROS) and cytosolic ROS (cROS) were detected through fluorescent dyes of MitoSOX and DCFH-DA (Right). Scale bar, 10 μm. Fluorescence intensity was analyzed by Image J. Columns: mean ± standard deviation (SD) of three independent experiments, $^{***}P < 0.001$. (C) The suppressed colony formation of LRPPRC-silenced T24 cells were rescued by the overexpression of circANKHD1. Data shown are the means ± SD of three experiments. $^{***}P < 0.001$. (D) Overexpression of circANKHD1 reversed the increased apoptosis cells resulting from LRPPRC knockdown. Data shown are the means ± SD of three experiments. $^{****}P < 0.0001$. (E) Western blot assay showed that overexpression of circANKHD1 reversed the up-regulated expression of the intrinsic apoptosis markers cleaved-caspase3, cleaved-caspase9, cleaved-PARP and BAX, and the down-regulated expression of BCL-2, without affecting the expression of caspase8. (F) Representative images of organoids derived from UCB patients treated with shNC, shLRPPRC or shLRPPRC-OE-circANKHD1, Scale bar, 100 μm (Top). qRT-PCR (Middle) and western blotting assays (Bottom, Left) validated that the LRPPRC-knockdown induced downexpression of FOXM1 was rescued after the over-expression of circANKHD1 in LRPPRC-silenced organoid UCB cells. qRT-PCR data are presented as fold change relative to NC organoids ±SD of three experiments, $^{****}P < 0.0001$. The suppressed proliferation of LRPPRC-silenced organoids was rescued by the overexpression of circANKHD1 (Bottom, Right). (G) Orthotopic xenograft bladder models implanted with LRPPRC-NC, LRPPRC-silenced or LRPPRC-silenced-OE-circANKHD1 T24 cells in Balb/c nude mice. The bioluminescent images of orthotopic xenograft bladder tumors were imaged by the IVIS 200 imaging system 6 weeks after cells were implanted (Left). The inhibition effect to orthotopic xenograft bladder tumors, induced by LRPPRC-deletion could be restored by overexpression of circANKHD1 *in vivo*. Data shown are the means ± SD, $^{**}P < 0.01$, $^{*}P < 0.05$. (For interpretation of the references to colour in this figure legend, the reader is referred to the Web version of this article.)

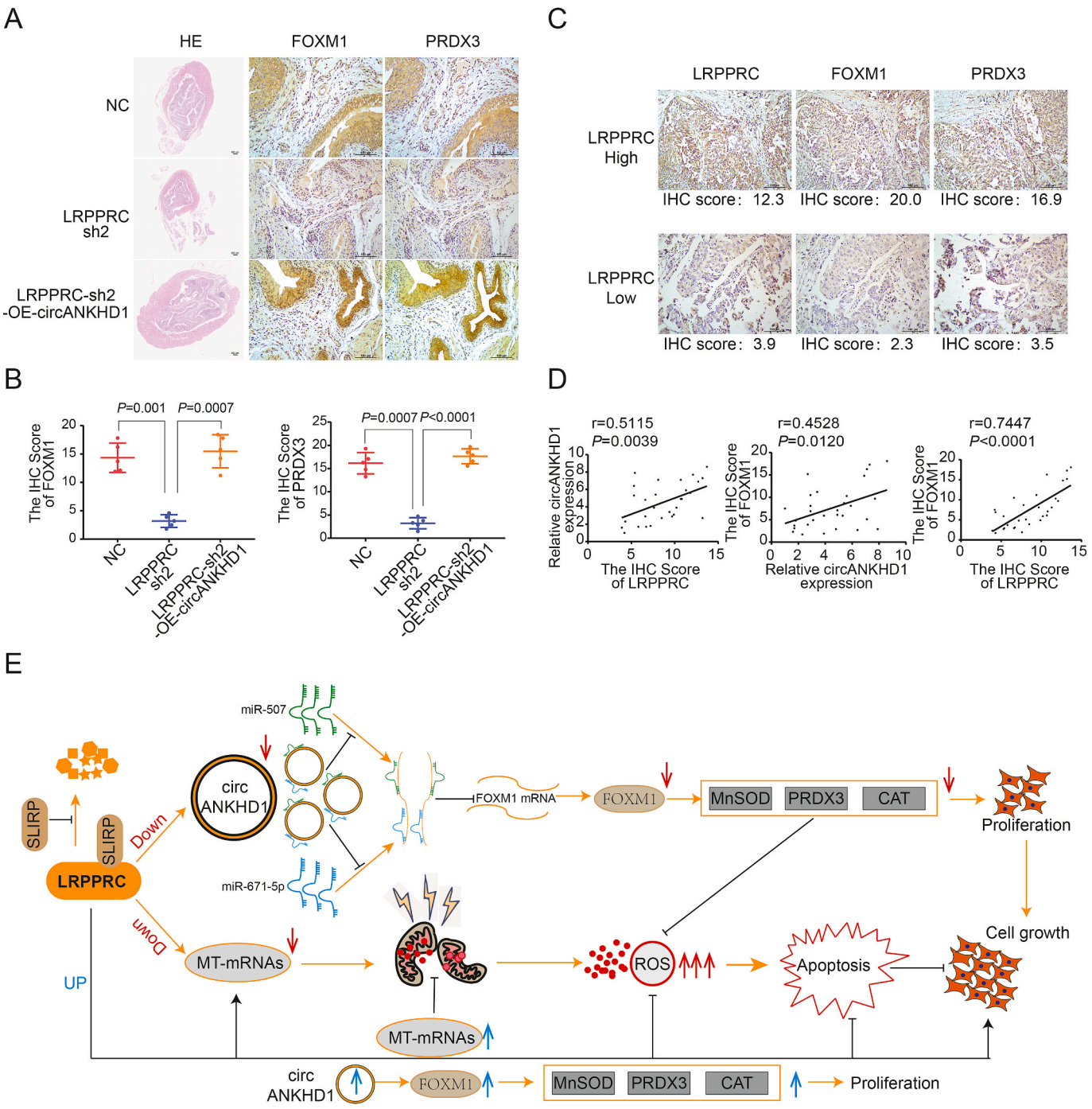

Fig. 7. LRPPRC regulates the circANKHD1/FOXM1 axis to promote cell growth in UCB. (A–B) The expression of FOXM1 and PRDX3 decreased after the knockdown of LRPPRC and were restored by the overexpression of circANKHD1 in orthotopic xenograft bladder tumors. Representative images of hematoxylin and eosin staining and IHC staining of FOXM1 and PRDX3 of orthotopic xenograft bladder tumors. Scale bar, 100 μm (A). IHC score of FOXM1 (Left) or PRDX3 (Right) in orthotopic xenograft bladder tumors as indicated. Data shown are the means ± SD, n = 5 (B). (C–D) The expression level of LRPPRC was positively correlated with that of circANKHD1 and FOXM1, and the expression level of circANKHD1 was positively correlated with that of FOXM1 in UCBs of the SYSUCC cohort. Representative images of IHC staining of LRPPRC, FOXM1 and PRDX3 in two UCB tissues with low or high expression of the three proteins. Scale bar, 100 μm (C). Spearman's correlation demonstrating that LRPPRC expression is positively correlated with circANKHD1 (detected by qRT-PCR) and FOXM1 (D). (E) Proposed model for the regulatory landscape of the LRPPRC/SLIPR/circANKHD1/FOXM1 signaling axis in promoting the pathogenesis of UCB. SLIRP forms a stable complex with LRPPRC to protect it from degradation, LRPPRC modulates ROS balance and protects UCB cells from oxidative stress via mt-mRNA metabolism and the circANKHD1/FOXM1 axis, thereby resulting in UCB cell growth.

cells were performed, and demonstrated that LRPPRC enhances the proliferation and inhibits the apoptosis of UCB cells; suggesting that LRPPRC protects UCB cells from oxidative stress by controlling the intracellular ROS homeostasis; and that LRPPRC promotes the growth of UCB cells both *in vitro* and *in vivo*.

To date, however, the molecular mechanisms by which LRPPRC regulates UCB cells' proliferation and apoptosis are largely unknown. Our results revealed that LRPPRC was closely associated with Ras GTPase binding, Ras protein signal transduction, ETC activity, OXPHOS, and the cell apoptosis signaling pathways. Based on KEGG and GO

analysis, our results revealed that LRPPRC was closely associated with ETC activity, respiratory chain and OXPHOS, all of which were correlated with the 13 ETC machinery proteins coded by mt-mRNAs [50]. Given that LRPPRC protein has been well characterized to acts as a global mt-mRNA chaperone enabling polyadenylation and translation [19,21], which is related to the pathway of ETC activity, respiratory chain and OXPHOS. Therefore, we focused on ETC activity, respiratory chain and OXPHOS pathways related to mitochondrial function for further research in our study.

Increasing evidence shows that mitochondria are of great importance for tumor growth as they regulate apoptosis and ROS production [9]. ROS are byproducts of oxidative respiration that can be generated either in the tricarboxylic acid (TCA) cycle or in the ETC [51,52]. There are 13 ETC machinery proteins coded by mitochondrial DNA (mtDNA), a small circular genome [50]. Dysregulation of mtRNA could result in alterations of mitochondrial proteins, which would influence ETC activity and lead to excess production of ROS [53,54]. Unexpectedly, we found that 12 mRNAs encoded by mtDNA and FOXM1 (which is a critical regulator of oxidative stress during oncogenesis [33]) were positively regulated by LRPPRC in UCB cells. This regulation of mt-mRNAs was validated by qRT-PCR in our T24-shLRPPRC cells. Control of intracellular ROS homeostasis is critical for cell proliferation and survival [10]. Consistent with the "ROS rheostat" theory, it has been suggested that low/medium levels of ROS enhance cell survival and lead to genetic instability, but excessive ROS levels result in stimulation of cell death pathways [11]. Because of increased cellular metabolism and activation of oncogenes, cancer cells generally produce relatively high levels of ROS, which makes tumor cells much more vulnerable to oxidative stress and more dependent on cellar antioxidant systems [33]. Our data revealed that the downregulation of LRPPRC greatly increased the cellular level of ROS, which might be related to the activation of the apoptosis pathway in UCB cells. Importantly, our study further demonstrated that FOXM1, a transcription factor that negatively regulates intracellular ROS levels [33], was also positively regulated by LRPPRC; strongly supporting the notion that LRPPRC is crucial for the regulation of ROS balance in UCB cells.

It has been reported that the transcription factor FOXM1 is frequently upregulated in most human malignancies [55]. FOXM1 is required for redox homeostasis and survival of cancer cells via the regulation of intracellular ROS levels [33,56,57]. Further studies have demonstrated that overexpression of FOXM1 not only accelerates cellular proliferation but also negatively regulates intracellular ROS levels by stimulating the expression of the detoxifying enzymes such as PRDX3, MnSOD and catalase [33,35]. In this present study, we observed that LRPPRC played an important role in the redox homeostasis of UCB cells. Our data suggested that the downregulation of LRPPRC-induced apoptosis was combined with excess accumulation of ROS in UCB cells. The results indicated that LRPPRC might regulate cell growth and apoptosis by regulating mt-mRNA and FOXM1 in UCB cells. Our results provided evidence that downregulation of LRPPRC not only disrupts ETC to lead to mitochondrial dysfunction, which can induce excess production of ROS, but also suppresses the detoxification of ROS via the downregulation of FOXM1 and its downstream ROS scavenger genes.

Until now, the LRPPRC protein has been well characterized to function as a global RNA chaperone that regulates the rate of mitochondrial protein synthesis and the stability of the poly (A) tails of mt-mRNAs [19]. LRPPRC/SLIRP complex acts as a global mt-mRNA chaperone to enable polyadenylation and translation [21]. Our data further showed that LRPPRC formed a stable complex with SLIRP, and SLIRP protected LRPPRC from degradation, which is consistent with previous studies [37,39]. However, the mechanisms by which LRPPRC regulates FOXM1 expression remain to be elucidated. LRPPRC is crucial for mRNA stability and acts as a global mRNA chaperone [21]. Nevertheless, little is known as to whether noncoding RNAs or small RNAs are regulated by LRPPRC. To better understand the regulatory mechanism of LRPPRC in UCB cells' ROS detoxification, we further performed a series of *in vitro* and *in vivo* studies. Our data showed that LRPPRC regulate the expression level of circANKHD1 in UCB cells; that circANKHD1 can regulate the expression level of FOXM1; and that circANKHD1 functionally acts as the sponge for miR-671-5p and miR-507, which suppresses the expression of FOXM1 in UCB cells. Furthermore, our correlation analysis showed a significantly positive correlation between the expression levels of LRPPRC and FOXM1 in UCB tissues. Taken together, we suggest that circANKHD1 might act as a linker between LRPPRC and FOXM1.

In the next part of this study, we revealed that silencing of LRPPRC induced an accumulation of ROS and inhibited the growth of UCB cells. These effects could be rescued by enforcing the overexpression of circANKHD1 both *in vitro* and *in vivo*. We further examined the positive relationship between LRPPRC and circANKHD1 expression in UCB tissues and cells, supporting the critical regulatory role in UCB cells' oxidative stress by the LRPPRC/circANKHD1 regulatory axis. Furthermore, our data showed that circANKHD1 was a critical positive regulator of FOXM1 and its downstream detoxifying enzymes. Downregulated expression of LRPPRC led to persistent accumulation of ROS induced by the downregulation of FOXM1 in UCB cells. These data suggest that LRPPRC may protect UCB from oxidative stress via the regulation of the circANKHD1/FOXM1 axis. In this study, we further demonstrated that FOXM1 is a novel target regulated by LRPPRC through circANKHD1, which could sponge miR-671-5p and miR-507 in UCB cells. These data, collectively, suggest a critical role of the LRPPRC/circANKHD1/FOXM1 axis in the control of UCB cells' redox homeostasis.

In summary, our study provides the first line of comprehensive evidence that LRPPRC is a potential therapy target as well as a prognostic biomarker in UCBs. LRPPRC exerts a bona fide regulatory role in stabilizing the function of mitochondrial ECT and promoting the circANKHD1/FOXM1 axis, thereby, regulating the redox homeostasis to support UCB cells' survival and tumorigenesis as illustrated in Fig. 7E. Thus, this study findings suggest LRPPRC as a novel therapeutic target for the treatment of human UCB.

Ethical approval and consent to participate

All the animal experiments were conducted according to the protocol approved by the Animal Care and Use Committee of Sun Yat-Sen University Cancer Center. This study was carried out in accordance with the institutional research ethics committee of Sun Yat-Sen University Cancer Center.

Consent for publication

Not applicable.

Availability of supporting data

In this study, the RNA-Seq data were deposited in the SRA database, and the Bioproject number is PRJNA771373, which includes SAMN22306813 and SAMN22306814.

Funding

This study was supported by grants from the National Natural Science Foundation of China, China 81972382 (F J. Zhou), and 81872091 (CP Yu)).

CPY, DX, ZWL and FJZ designed the study. WSW, ZWL. DX, and CPY designed the experiments and analysis. WSW, NW, MHD, PD, JYL, ZX, ZHL, YLP, ZL. WHL and YLY carried out the experiments. WSW, PD, XDL, ZYL, LJJ and KY performed bioinformatics and statistical analysis. WSW, NW, MHD, PD and ZLZ analyzed the data. CPY supervised the research and, together with WSW, PD, and JYL wrote the manuscript. All authors have read and approved the final version of the manuscript.

Declaration of competing interest

The authors declare that they have no competing interests.

Acknowledgements

We are thankful to the TCGA research network for providing the data used in our study. We are grateful to the patients and mice for their contributions and sacrifices to this study.

Appendix A. Supplementary data

Supplementary data to this article can be found online at https://doi.org/10.1016/j.redox.2021.102201.

References

[1] F. Bray, J. Ferlay, I. Soerjomataram, R.L. Siegel, L.A. Torre, A. Jemal, Global cancer statistics 2018: GLOBOCAN estimates of incidence and mortality worldwide for 36 cancers in 185 countries, CA A Cancer J. Clin. 68 (6) (2018) 394–424.
[2] M. Burger, J.W. Catto, G. Dalbagni, H.B. Grossman, H. Herr, P. Karakiewicz, et al., Epidemiology and risk factors of urothelial bladder cancer, Eur. Urol. 63 (2013) 234–241.
[3] O. Sanli, J. Dobruch, M.A. Knowles, M. Burger, M. Alemozaffar, M.E. Nielsen, et al., Bladder cancer, Nat. Rev. Dis. Primers 3 (2017) 17022.
[4] B. Jordan, J.J. Meeks, T1 bladder cancer: current considerations for diagnosis and management, Nat. Rev. Urol. 16 (2019) 23–34.
[5] F. Massari, M. Santoni, C. Ciccarese, M. Brunelli, A. Conti, D. Santini, et al., Emerging concepts on drug resistance in bladder cancer: implications for future strategies, Crit. Rev. Oncol. Hematol. 96 (2015) 81–90.
[6] H.M. Huang, H.X. Li, Tumor heterogeneity and the potential role of liquid biopsy in bladder cancer, Cancer Commun. 41 (2021) 91–108, https://doi.org/10.1002/cac2.12129.
[7] J. Afonso, L.L. Santos, A. Longatto-Filho, F. Baltazar, Competitive glucose metabolism as a target to boost bladder cancer immunotherapy, Nat. Rev. Urol. 17 (2020) 77–106.
[8] K. Vasan, M. Werner, N.S. Chandel, Mitochondrial metabolism as a target for cancer therapy, Cell Metabol. 32 (2020) 341–352.
[9] S. Vyas, E. Zaganjor, M.C. Haigis, Mitochondria and cancer, Cell 166 (2016) 555–566.
[10] D. Anastasiou, G. Poulogiannis, J.M. Asara, M.B. Boxer, J.K. Jiang, M. Shen, et al., Inhibition of pyruvate kinase M2 by reactive oxygen species contributes to cellular antioxidant responses, Science 334 (2011) 1278–1283.
[11] M. Maryanovich, A. Gross, A ROS rheostat for cell fate regulation, Trends Cell Biol. 23 (2013) 129–134.
[12] R.N. Lightowlers, Z.M. Chrzanowska-Lightowlers, Human pentatricopeptide proteins: only a few and what do they do, RNA Biol. 10 (2013) 1433–1438.
[13] O. Rackham, A. Filipovska, The role of mammalian PPR domain proteins in the regulation of mitochondrial gene expression, Biochim. Biophys. Acta 1819 (2012) 1008–1016.
[14] I. Kühl, C. Kukat, B. Ruzzenente, D. Milenkovic, A. Mourier, M. Miranda, et al., POLRMT does not transcribe nuclear genes, Nature 514 (2014) E7–E11.
[15] I. Kühl, M. Miranda, V. Posse, D. Milenkovic, A. Mourier, S.J. Siira, et al., POLRMT regulates the switch between replication primer formation and gene expression of mammalian mtDNA, Sci. Adv. 2 (2016), e1600963.
[16] J. Holzmann, P. Frank, E. Löffler, K.L. Bennett, C. Gerner, W. Rossmanith, RNase P without RNA: identification and functional reconstitution of the human mitochondrial tRNA processing enzyme, Cell 135 (2008) 462–474.
[17] O. Rackham, J.D. Busch, S. Matic, S.J. Siira, I. Kuznetsova, I. Atanassov, et al., Hierarchical RNA processing is required for mitochondrial ribosome assembly, Cell Rep. 16 (2016) 1874–1890.
[18] O. Rackham, S.M. Davies, A.M. Shearwood, K.L. Hamilton, J. Whelan, A. Filipovska, Pentatricopeptide repeat domain protein 1 lowers the levels of mitochondrial leucine tRNAs in cells, Nucleic Acids Res. 37 (2009) 5859–5867.
[19] B. Ruzzenente, M.D. Metodiev, A. Wredenberg, A. Bratic, C.B. Park, Y. Cámara, et al., LRPPRC is necessary for polyadenylation and coordination of translation of mitochondrial mRNAs, EMBO J. 31 (2012) 443–456.
[20] F. Sasarman, C. Brunel-Guitton, H. Antonicka, T. Wai, E.A. Shoubridge, LSFC Consortium, LRPPRC and SLIRP interact in a ribonucleoprotein complex that regulates posttranscriptional gene expression in mitochondria, Mol. Biol. Cell 21 (2010) 1315–1323.
[21] S.J. Siira, H. Spåhr, A.J. Shearwood, B. Ruzzenente, N.G. Larsson, O. Rackham, et al., LRPPRC-mediated folding of the mitochondrial transcriptome, Nat. Commun. 8 (2017) 1532.
[22] S.M. Davies, M.I. Lopez Sanchez, R. Narsai, A.M. Shearwood, M.F. Razif, I.D. Small, et al., MRPS27 is a pentatricopeptide repeat domain protein required for the translation of mitochondrially encoded proteins, FEBS Lett. 586 (2012) 3555–3561.
[23] S.M. Davies, O. Rackham, A.M. Shearwood, K.L. Hamilton, R. Narsai, J. Whelan, et al., Pentatricopeptide repeat domain protein 3 associates with the mitochondrial small ribosomal subunit and regulates translation, FEBS Lett. 583 (2009) 1853–1858.
[24] T. Zhou, Y.H. Sang, S. Cai, C. Xu, M.H. Shi, The requirement of mitochondrial RNA polymerase for non-small cell lung cancer cell growth, Cell Death Dis. 12 (2021) 751.
[25] J. Cui, L. Wang, X. Ren, Y. Zhang, H. Zhang, LRPPRC: a multifunctional protein involved in energy metabolism and human disease, Front. Physiol. 10 (2019) 595.
[26] T. Tian, J. Ikeda, Y. Wang, S. Mamat, W. Luo, K. Aozasa, et al., Role of leucine-rich pentatricopeptide repeat motif-containing protein (LRPPRC) for anti-apoptosis and tumourigenesis in cancers, Eur. J. Cancer 48 (2012) 2462–2473.
[27] W.S. Wei, X. Chen, L.Y. Guo, X.D. Li, M.H. Deng, G.J. Yuan, et al., TRIM65 supports bladder urothelial carcinoma cell aggressiveness by promoting ANXA2 ubiquitination and degradation, Cancer Lett. 435 (2018) 10–22.
[28] J.Y. Chan, J.Q. Lim, J. Yeong, V. Ravi, P. Guan, A. Boot, et al., Multiomic analysis and immunoprofiling reveal distinct subtypes of human angiosarcoma, J. Clin. Invest. 130 (2020) 5833–5846.
[29] C. Mascaux, M. Angelova, A. Vasaturo, J. Beane, K. Hijazi, G. Anthoine, et al., Immune evasion before tumour invasion in early lung squamous carcinogenesis, Nature 571 (2019) 570–575.
[30] J.S. Park, C.J. Burckhardt, R. Lazcano, et al., Mechanical regulation of glycolysis via cytoskeleton architecture, Nature 578 (2020) 621–626, https://doi.org/10.1038/s41586-020-1998-1.
[31] N.N. Pavlova, C.B. Thompson, The emerging hallmarks of cancer metabolism, Cell Metabol. 23 (2016) 27–47.
[32] L. Valcarcel-Jimenez, E. Gaude, V. Torrano, C. Frezza, A. Carracedo, Mitochondrial metabolism: Yin and Yang for tumor progression, Trends Endocrinol. Metabol. 28 (2017) 748–757.
[33] H.J. Park, J.R. Carr, Z. Wang, V. Nogueira, N. Hay, A.L. Tyner, et al., FoxM1, a critical regulator of oxidative stress during oncogenesis, EMBO J. 28 (2009) 2908–2918.
[34] G.S. Shadel, T.L. Horvath, Mitochondrial ROS signaling in organismal homeostasis, Cell 163 (2015) 560–569.
[35] H.J. Choi, Y.L. Jhe, J. Kim, J.Y. Lim, J.E. Lee, M.K. Shin, et al., FoxM1-dependent and fatty acid oxidation-mediated ROS modulation is a cell-intrinsic drug resistance mechanism in cancer stem-like cells, Redox Biol. 36 (2020) 101589.
[36] R.J. DeBerardinis, N.S. Chandel, Fundamentals of cancer metabolism, Sci. Adv. 2 (2016), e1600200.
[37] M. Lagouge, A. Mourier, H.J. Lee, H. Spåhr, T. Wai, C. Kukat, et al., SLIRP regulates the rate of mitochondrial protein synthesis and protects LRPPRC from degradation, PLoS Genet. 11 (2015), e1005423.
[38] W. Zhou, G. Sun, Z. Zhang, L. Zhao, L. Xu, H. Yuan, et al., Proteasome-independent protein knockdown by small-molecule inhibitor for the undruggable lung adenocarcinoma, J. Am. Chem. Soc. 141 (2019) 18492–18499.
[39] H. Spåhr, A. Rozanska, X. Li, I. Atanassov, R.N. Lightowlers, Z.M. Chrzanowska-Lightowlers, et al., SLIRP stabilizes LRPPRC via an RRM-PPR protein interface, Nucleic Acids Res. 44 (2016) 6868–6882.
[40] T.B. Hansen, T.I. Jensen, B.H. Clausen, J.B. Bramsen, B. Finsen, C.K. Damgaard, et al., Natural RNA circles function as efficient microRNA sponges, Nature 495 (2013) 384–388.
[41] V. Agarwal, G.W. Bell, J.W. Nam, D.P. Bartel, Predicting effective microRNA target sites in mammalian mRNAs, Elife 4 (2015).
[42] J. Ding, X. Li, H. Hu, TarPmiR: a new approach for microRNA target site prediction, Bioinformatics 32 (2016) 2768–2775.
[43] S. Yang, X. He, J. Zhao, et al., Mitochondrial transcription factor A plays opposite roles in the initiation and progression of colitis-associated cancer, Cancer Commun. (2021) 41 695–714, https://doi.org/10.1002/cac2.12184.
[44] W. Gao, J. Xua, F. Wang, L. Zhang, R. Peng, Y. Zhu, et al., Mitochondrial proteomics approach reveals voltage-dependent anion channel 1 (VDAC1) as a potential biomarker of gastric cancer, Cell. Physiol. Biochem. 37 (2015) 2339–2354.
[45] X. Jiang, X. Li, H. Huang, F. Jiang, Z. Lin, H. He, et al., Elevated levels of mitochondrion-associated autophagy inhibitor LRPPRC are associated with poor prognosis in patients with prostate cancer, Cancer 120 (2014) 1228–1236.
[46] X. Jiang, W. Zhong, H. Huang, H. He, F. Jiang, Y. Chen, et al., Autophagy defects suggested by low levels of autophagy activator MAP1S and high levels of autophagy inhibitor LRPPRC predict poor prognosis of prostate cancer patients, Mol. Carcinog. 54 (2015) 1194–1204.
[47] X. Li, L. Lv, J. Zheng, J. Zhou, B. Liu, H. Chen, et al., The significance of LRPPRC overexpression in gastric cancer, Med. Oncol. 31 (2014) 818.
[48] T. Nishio, N. Kurabe, N. Goto-Inoue, T. Nakamura, H. Sugimura, M. Setou, et al., Immunohistochemical expression analysis of leucine-rich PPR-motif-containing protein (LRPPRC), a candidate colorectal cancer biomarker identified by shotgun proteomics using iTRAQ, Clin. Chim. Acta 471 (2017) 276–282.
[49] H.Y. Zhang, Y.D. Ma, Y. Zhang, J. Cui, Z.M. Wang, Elevated levels of autophagy-related marker ULK1 and mitochondrion-associated autophagy inhibitor LRPPRC are associated with biochemical progression and overall survival after androgen deprivation therapy in patients with metastatic prostate cancer, J. Clin. Pathol. 70 (2017) 383–389.
[50] B. Schöpf, H. Weissensteiner, G. Schäfer, F. Fazzini, P. Charoentong, A. Naschberger, et al., OXPHOS remodeling in high-grade prostate cancer involves mtDNA mutations and increased succinate oxidation, Nat. Commun. 11 (2020) 1487.
[51] D.L. Galvan, N.H. Green, F.R. Danesh, The hallmarks of mitochondrial dysfunction in chronic kidney disease, Kidney Int. 92 (2017) 1051–1057.
[52] H. Nohl, A.V. Kozlov, L. Gille, K. Staniek, Cell respiration and formation of reactive oxygen species: facts and artefacts, Biochem. Soc. Trans. 31 (2003) 1308–1311.

[53] D. Grasso, L.X. Zampieri, T. Capelôa, J.A. Van de Velde, P. Sonveaux, Mitochondria in cancer, Cell Stress 4 (2020) 114–146.
[54] V. Raimondi, F. Ciccarese, V. Ciminale, Oncogenic pathways and the electron transport chain: a dangeROS liaison, Br. J. Cancer 122 (2020) 168–181.
[55] A.L. Gartel, FOXM1 in cancer: interactions and vulnerabilities, Cancer Res. 77 (2017) 3135–3139.
[56] M. Halasi, B. Pandit, M. Wang, V. Nogueira, N. Hay, A.L. Gartel, Combination of oxidative stress and FOXM1 inhibitors induces apoptosis in cancer cells and inhibits xenograft tumor growth, Am. J. Pathol. 183 (2013) 257–265.
[57] I.S. Song, Y.J. Jeong, S.H. Jeong, H.J. Heo, H.K. Kim, K.B. Bae, et al., FOXM1-Induced PRX3 regulates stemness and survival of colon cancer cells via maintenance of mitochondrial function, Gastroenterology 149 (2015) 1006–1016. e9.